Thermal control architecture for planetary and lunar (sub-)surface exploration robots

THERMAL CONTROL ARCHITECTURE FOR PLANETARY AND LUNAR (SUB-)SURFACE EXPLORATION ROBOTS

by
Brian Burg

Diploma Thesis at the
Eidgenössische Technische Hochschule, Zurich (ETH)

Advisors:

Prof. Dr. Steven Dubowsky
Field and Space Robotics Laboratory
Massachusetts Institute of Technology (MIT)

Prof. Dr. John H. Lienhard V
W. M. Rohsenow Heat and Mass Transfer Laboratory
Massachusetts Institute of Technology (MIT)

Prof. Dr. Dimos Poulikakos
Laboratory of Thermodynamics in Emerging Technologies
Eidgenössische Technische Hochschule, Zurich (ETH)

March 2006

What the hell, it works on Star Trek.
Skroob in *Spaceballs (1987)*

Abstract

A thermal control architecture design study is conducted on a novel robotic planetary and lunar (sub-)surface exploration paradigm. The concept is based on the deployment of a large number of small spherical fuel cell powered robots over vast areas, which employ hopping, bouncing and rolling as locomotion mode. The aim of the research is to prevent freezing and overheating of the robots, without compromising mechanical and thermal reliability and stability. A first order thermal model approximation is evaluated for all possible mission locations and predictions with respect to expected heat loss and lifetime are made. The proposed thermal control architecture, relying on a low emissive silver coating surface finish and low conductive silica aerogel insulation layer, enables a single design to be employed on all envisioned mission destinations, as the projected heat loss never surpasses internal heat generation. The effects of a thermal control heat rejection mechanism, composed of a variable emittance coating and heat switch, in order to increase mission flexibility, are also studied from a thermal standpoint.

Acknowledgments

This work was carried out at the Rohsenow Heat and Mass Transfer Laboratory, part of the Department for Mechanical Engineering at the Massachusetts Institute of Technology (MIT).

I would like to express my sincere thanks to Prof. Dr. Dimos Poulikakos, head of the Laboratory of Thermodynamics in Emerging Technologies at the Eidgenössische Technische Hochschule, Zurich (ETH), for supervising this thesis, his incitement for it to be written at MIT and arranging its realization.

I feel deeply grateful to Prof. Dr. John H. Lienhard V, from the Rohsenow Heat and Mass Transfer Laboratory at MIT, for his commitment to advising the thesis, his personnel support and encouragement during the whole time, the constructive discussion together and especially his extremely valuable and always accessible guidance.

Furthermore I would like to thank Prof. Dr. Steven Dubowsky, head of the Field and Space Robotics Laboratory at MIT, for initializing the project and providing helpful assistance by making useful and practical suggestions all throughout the work.

Last but not least I would like to thank Dr. Jean-Sébastien Plante, Samuel Kesner and Lauren DeVita for being constant and reliable sources in solving and evaluating design specific challenges, and for their personal advice during the entire course of the study, which was greatly appreciated.

Contents

Chapter 1

Introduction

When *Science* (2005, [1]) announced its *Breakthrough of the Year* in 2005, planetary and space scientists and engineers found themselves awarded the runners-up position because they *"outdid themselves (...) in mounting exploratory expeditions beyond Earth"*.

1.1 The Vision for Space Exploration

Much of this work is based upon the United States National Aeronautics and Space Administration's (NASA) *The Vision for Space Exploration* (2004, [2]) in addition to projects from the European Space Agency (ESA) and the Japan Aerospace Exploration Agency (JAXA).

The Vision for Space Exploration is a framework for exploring our solar system, seeking answers to profound scientific questions, responding to recent discoveries and implementing revolutionary technologies. Today spacecraft are at or on their way to the Moon, Mercury, Venus, Mars, a comet, an asteroid, Saturn, Pluto and the very edge of the solar system.

To encourage outside thinkers and researchers to take part in this enterprise, NASA created the NASA Institute for Advanced Concepts (NIAC), which seeks proposals for revolutionary aeronautics and space concepts that could dramatically impact how NASA develops and conducts its missions.

1.1.1 NASA Institute for Advanced Concepts (NIAC)

While NIAC (2004, [3]) seeks advanced concept proposals that stretch the imagination, these concepts have to be based on sound scientific principles and attainable within a 10 to 40-year time frame.

To achieve this goal NIAC calls for proposals pursuing these aims and is entitled to fund studies based on acceptance. In a first phase, lasting 6 months, \$75˙000 are granted for a more in depth study of the proposal. If the concept proves to be promising, in a second phase, lasting as long as 2 years, up to \$400˙000 can be granted before the project is handed over from NIAC to NASA.

Since its establishment in 1998 through 2005, NIAC has received a total of 1˙016 proposals and has awarded 115 Phase I grants and 32 Phase II contracts for a total value of \$22.5 million.

1.2 Robots for Celestial Body Surface and Subsurface Exploration

A new mission concept for celestial body exploration, based on the deployment of a large number of small (meso-scale) spherical mobile robots over vast areas of a celestial body's surface and subsurface, is being investigated by Dubowsky *et al.* (2005, [4]) and is funded as a NIAC Phase II project.

This strategic exploration architecture enables large-scale in situ analysis of scientifically interesting properties, thus enabling a new paradigm for solar system wide exploration, mapping and scientific study. The approach is an important alternative to current rover and lander-based planetary exploration, which is limited to studying small areas of a celestial body surface. Once developed, robot units can be custom-tailored to specific mission targets.

In the study, a detailed mission scenario will be developed, enabling technologies for actuation, power, sensing and communication surveyed and fundamental research on the robot mobility mechanisms undertaken. This includes the manufacturing of a small number of prototypes which will be tested in field conditions. Work will be conducted by a multi-university team of engineers and scientists at MIT, New Mexico Institute of Mining & Technology and Stanford.

Research objective

The focus of this work lies in the thermal control architecture design of these exploration robots, to enable autonomous operation without risking freezing or overheating damage of robot components in harsh space mission conditions.

Chapter 2

Literature Review

2.1 Robot System Description

The proposed mission concept (Dubowsky *et al.* 2005, [4]) is based on the deployment of a large number (hundreds to thousands) of cm-scale mobile robots over very large areas of a celestial body's surface and subsurface by orbital craft, from aerial platforms or a lander. The exploration robot is a self-contained spherical robot equipped with power and communication systems, a mobility system that enables it to move via hopping, rolling and bouncing, and a suite of miniaturized sensors such as imagers, spectrometers and sensors for chemical analysis. A first conceptual design is seen in Figure 2.1.

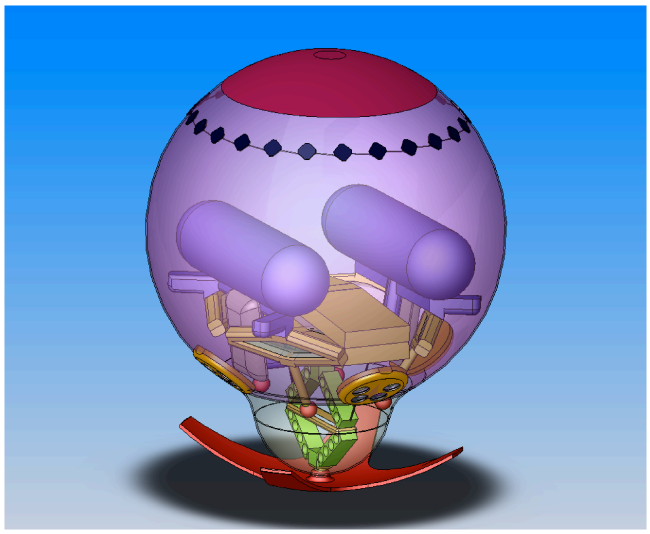

Figure 2.1: Conceptual design of exploration robot

Since many robots will be deployed, the overall system is highly redundant and robust. Significant losses of units will not jeopardize mission goals.

2.1.1 Mobility

By combining hopping, rolling and bouncing, an effective displacement method for small devices in low gravity is found. This locomotion mode will allow the robots to travel through extremely rough terrain and access sites of interest that are beyond the reach of ordinary rovers and orbital or aerial platforms, such as icy terrains on polar Mars, various gas giant moons, rough and vertical relief landscapes and caves or other subsurface areas.

Basic robot mobility is provided by a bistable mechanism activated by dielectric elastomer actuators, also known as electroactive polymer muscle actuators (EPAM). The device allows a continuous transducer charging with an instant energy release. EPAMs have shown to be potentially highly efficient, low cost, light weight and inherently simple. The operating principle is based on the Maxwell (electrostatic) pressure, generated by a strong electric field applied across a soft elastomeric material and is shown in Figure 2.2.

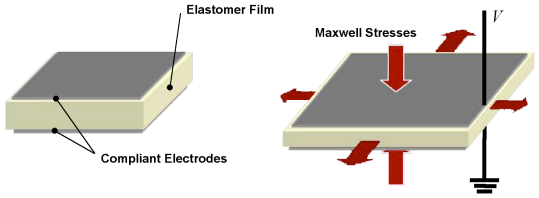

Figure 2.2: Dielectric elastomer actuator operating principle

The bistable mechanism enables the robots to achieve mobility via directed hopping and they are weighted so that after one locomotion cycle of hopping, rolling and bouncing they will return to a posture with their "foot" on the ground. An overview of the bistable system concept is given in Figure 2.3.

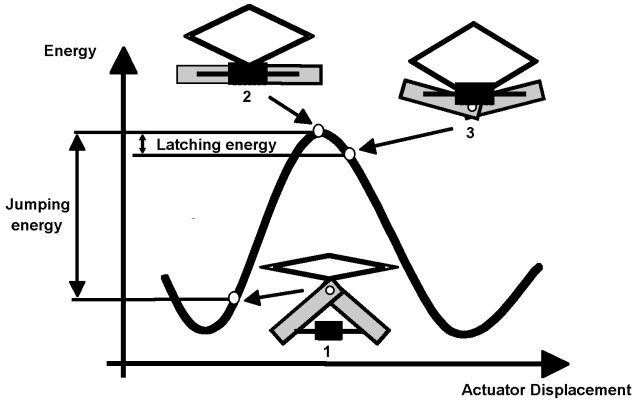

Figure 2.3: Bistable actuator mobility system concept

2.1.2 Power

The units will be powered by a miniaturized fuel cell concept, developed in connection with O'Hayre *et al.* (2003, [5]) from Stanford University, as they lack the surface area for conventional photo-voltaic cells on remote celestial bodies and would not qualify for subsurface missions in that case. Analyses have shown that fuel cell powered robots offer significant mass reduction advantages for long range missions over similar battery powered units. The use of bistable mechanisms for the EPAM actuators, which lowers peak power consumption necessary for hopping, justifies the use of high efficiency - low power devices such as fuel cells.

2.1.3 Sensors

Sensors are the heart of the exploration robots as they perform all aspects of scientific exploration, tailored to specific mission objectives. Additionally, the robots will also require sensors related to navigation, localization and locomotion, such as accelerometers and gyroscopes. Ideally all sensors are to be incorporated into Micro Electro-Mechanical Systems (MEMS), to reduce size, weight, cost and power consumption.

2.1.4 Communication

Science data will be transmitted via low-power communication to a lander platform or an orbiting spacecraft, which then relays the data to Earth. Individual robots will cooperate semi-autonomously to share information, collaboratively explore science targets and relay commands and data in caves. Individual units form a local area network (LAN) to allow communication by a low-power transmission/receiver system.

2.2 Reference Missions

2.2.1 Surface Reference Mission

The surface reference mission envisions exploration of a body having solid terrain. The surface roughness is assumed to be very high, consisting of dense rock distributions, steeply sloped terrain features such as gullies and escarpments, loose drift material with hazardous mobility characteristics and small-scale unevenness caused by small rocks, pebbles etc. Such terrain is often of primary interest to planetary scientists, due to the possibility of exposed volatiles in wind or water-formed geological features. Targets include lava flows, chaotic or fractured terrain, cliffs, rock overhangs, tafoni, impact fracture fields, dunes and polygonal or other periglacial terrain (Dubowsky *et al.* 2005, [4]).

2.2.2 Subsurface Reference Mission

The subsurface reference mission envisions exploration of cave-like subterranean regions, formed by volcanic action (i.e. lava tube caves). The cave floor is assumed to be relatively flat in its interior, due to the nature of its volcanic formation. Near surface entrances, rubble from collapsed rock formations that

created the entrances, has been leveled by layers of sediment, accumulated over millions (or even billions) of years. The cave profile will include both inclined an declined slopes that the exploration robots must traverse. Lava tubes are found on Mars, the Moon, Venus and Io. Icy caves are thought to exist in Martian poles, icy moons and sublimation cavities in comet interiors.

These targets are valuable since natural caves and other subsurface voids provide a radically different set of conditions than the overlying surface. Such areas serve as repository for trapped materials from a planet's past and yield materials that may shed light on past climate history and past solar activity. They can also provide a suite of environments for an enormous diversity of extremophile organisms and have been suggested as the last refuge of life on planets like Mars, where surface conditions have become significantly less hospitable to life over geological time (Dubowsky *et al.* 2005, [4]).

2.3 Possible Mission Locations

NASA's *The Vision for Space Exploration* (2004, [2]) cites several goals and objectives for space exploration beyond low Earth orbit. They include in particular the exploration of the following celestial bodies:

- The Moon
- Mars
- Jupiter's Galilean moons Io, Europa, Ganymede and Callisto
- Saturn's moon Titan
- Asteroids and other bodies

The aim is to understand the history of our solar system, to search for evidence of life and to develop new technologies for power generation, propulsion, life support and other key capabilities required to support more distant, more capable and longer duration exploration missions. All these bodies appear to be the most promising in reaching these ambitions and intentions.

2.4 Demands and Conditions on Probable Mission Locations

So far, no choice of definite mission destinations has been made for the proposed exploration robots. In a first step it is therefore important to know the near surface conditions of all possible mission locations in order to evaluate their suitability as potential robot exploration object.

The factors that determine the qualification of a celestial for body being in principle eligible as robotic exploration mission destination are temperature, pressure and gravitational acceleration. The maximum temperature may not exceed allowable temperatures of any robot component, which in a first approach is considered to be in the order of 50°C. The highest acceptable pressure may not differ substantially from Earth atmospheric pressure of 1 bar. Gravitational acceleration must further be high enough to meet mobility demands and exceed at least 0.7–1 m/s^2. All numbers are referenced to traditionally designed, non cooling low cost robots, as proposed in the project.

The information collected for each in question coming celestial body is described in Tables 2.1 to 2.16. A first useful number is the radius of the body to get an impression on its size. Gravitational acceleration is stated next. The rotation period of the celestial body accounts for the length of a day. The respective units of hours and days are related to Earth. From this value the average solar irradiation duration can be estimated. The intensity of solar irradiation is derived from the distance to the sun, also known as semi-major axis. It is given in Astronomical Units (AU), which are defined in Equation 2.1.

$$1 \text{ AU} = 1.4960 \cdot 10^{11} \text{ km} \tag{2.1}$$

This equals the distance from the sun to Earth.

The observed temperature, along with any additional observations made regarding temperatures on the celestial body, are mentioned in the following. Finally the atmospheric pressure, together with its major elements of composition and knowledge on surface material and morphology is given.

All data is found in Weismann *et al.* (1999, [6]), unless noted elsewise. In this case it is taken from McBride and Gilmour (2004, [7]).

The general framework for a specific robot thermal control architecture design is based upon the conditions prevailing in the operation area. This allows a model to be simulated and evaluate robot behavior in different conditions, in order to infer its applicability in the investigated surroundings.

Before though advanced robotic missions are conducted to study various celestial bodies, specific knowledge for mission planning related purposes is required, which only can be gathered through a prior orbiting spacecraft mission. This aspect will be covered in more detail in Section 6.2.

2.4.1 Planets

Only planets in our solar system made up of a solid surface without a dense atmosphere come into question to serve as exploration destination for the robots.

First planet of the solar system is Mercury and its information of interest for thermal design considerations is written down in Table 2.1.

Mercury			
Radius:	2439 km	Gravity:	3.7 m/s^2 [7]
Rotation Period:	58.6 days	Semi-major Axis:	0.39 AU
Temperature Range:	90–725 K	Poles:	<135 K
Atmospheric Pressure:	fbar	Composition:	H, He, O_2
Surface Material and Morphology:		Regolith, heavily cratered	

Table 2.1: Mercury surface conditions

Extremely high temperatures in equatorial areas, resulting from Mercury's short distance to the sun, prohibit the use of traditionally designed robots for exploration purposes. Much lower temperatures on the poles however allow these regions to be envisioned for mission destinations.

Data for Venus, the closest planet to Earth, is noted in Table 2.2.

Venus			
Radius:	6051 km	Gravity:	8.9 m/s^2
Rotation Period:	243 days	Semi-major Axis:	0.72 AU
Mean Temperature:	730 K	(green house effects)	
Atmospheric Pressure:	90±2 bar	Composition:	CO_2, N_2
Surface Material and Morphology:		Mosaic of volcanic planes	

Table 2.2: Venus surface conditions

Due to high temperatures, caused by atmospheric green house effects, and high atmospheric pressures, Venus does not qualify for exploration by the proposed types of robots.

For reference purposes and considerations to be made during the design and manufacturing of a prototype, the same relevant data for Earth is given in Table 2.3.

Earth			
Radius:	6378 km	Gravity:	9.8 m/s^2
Rotation Period:	23.9 hours	Semi-major Axis:	1.00 AU
Temperature Range:	223–323 K	Mean:	288 K
Atmospheric Pressure:	1 bar	Composition:	N_2, O_2
Surface Material and Morphology:		Continents and oceans	

Table 2.3: Earth surface conditions

Mars, the fourth planet of our solar system is by far the best studied planet, due to numerous missions flown there. Very detailed information for near surface conditions in known, as published by Martin *et al.* (2003, [8]) and even an atmospheric circulation model developed by Haberle *et al.* (1999, [9]) exists. All necessary information for present purposes is found in Table 2.4.

Mars			
Radius:	3396 km	Gravity:	3.7 m/s^2
Rotation Period:	24.6 hours	Semi-major Axis:	1.52 AU
Temperature Range:	180–290 K	Poles:	150 K
Atmospheric Pressure:	0.3–14 mbar	Composition:	CO_2, N_2
Surface Material and Morphology:		Crust with deformations	

Table 2.4: Mars surface conditions

It is needless to say, that Mars is suitable and remains a target of high interest for planetary exploration.

The giant gas planets of the solar system Jupiter, Saturn, Uranus and Neptune possess a much too dense atmosphere for robotic exploration missions, as their reference name anticipates.

Information for Pluto, the last planet of the solar system is contained in Table 2.5.

Pluto			
Radius:	1170 km	Gravity:	0.7 m/s^2
Rotation Period:	6.4 days	Semi-major Axis:	39.48 AU
Temperature Range:	40–60 K		
Atmospheric Pressure:	<60 mbar	Composition:	N_2
Surface Material and Morphology:		Variegated surface, polar regions	

Table 2.5: Pluto surface conditions

At first sight, Pluto appears to be suited for a robotic exploration mission. The large distance from Earth and low gravity must however be taken into account during mission planning.

2.4.2 Natural Satellites

Neither Mercury, nor Venus posses any natural satellites.

The Earth's Moon has emerged as a site of interest for robot surface exploration missions due to the renewed desire to conduct human exploration missions there. The envisioned robotic missions should prepare and support future human exploration activities. Relevant data is collected in Table 2.6.

Moon (Earth)			
Radius:	1738 km	Gravity:	1.6 m/s^2 [7]
Rotation Period:	27.3 days		
Temperature Range:	104–390 K		
Atmospheric Pressure:	fbar	Composition:	H, He, Ne
Surface Material and Morphology:		Regolith (Moon soil)	

Table 2.6: Moon surface conditions

Even though maximal temperatures may be considered too high at certain latitudes, the long rotation period allows exploration missions to be exclusively conducted at a specific time of day. On latitudes closer to the poles the maximal temperatures are also considerably lower.

Phobos and Deimos are the two moons of Mars and their respective information is found in Tables 2.7 and 2.8.

Phobos (Mars)			
Radius:	11 km [7]	Gravity:	0.3–0.6 m/s^2
Rotation Period:	7.6 hours		
Temperature Range:	n/a		
Atmospheric Pressure:	n/a	Composition:	n/a
Surface Material and Morphology:		Similar to Moon and asteroids	

Table 2.7: Phobos surface conditions

Deimos (Mars)			
Radius:	6 km [7]	Gravity:	0.2–0.3 m/s^2
Rotation Period:	30.3 hours		
Temperature Range:	n/a		
Atmospheric Pressure:	n/a	Composition:	n/a
Surface Material and Morphology:		Similar to Moon and asteroids	

Table 2.8: Deimos surface conditions

Due to their small size and resulting low gravity, Phobos and Deimos do not qualify for this type of mission, because the mobility of the hopping robots can not be sufficiently controlled.

Jupiter has at least 63 moons. The four largest moons, known as "Galilean Moons" are Io, Europa, Ganymede and Callisto in order from closest to farthest away from Jupiter.

Io, the innermost of the Galilean moons, is of high interest for space exploration, due to its volcanic activity and extremely high localized temperatures. Information related to Io is in Table 2.9 and some data stems from NASA's Jet Propulsion Laboratory (JPL) (2005, [10]). Because of colder areas apart from volcanos, it can be envisioned to dispatch probing missions there.

Io (Jupiter)			
Radius:	1821 km	Gravity:	1.8 m/s^2
Rotation Period:	1.8 days		
Temperature Range:	135–300 K [10]	Volcanos:	1800 K
Atmospheric Pressure:	nbar, pbar	Composition:	SO_2, SO
Surface Material and Morphology:		Volcanic plains, SO_2 frost	

Table 2.9: Io surface conditions

The other Galilean moons, known as Icy Moons, are also suitable for robot exploration. Their data is summarized in Tables 2.10 to 2.12. Some data sources are again provided by JPL (2005, [11], [12], [13]).

Europa (Jupiter)			
Radius:	1560 km	Gravity:	1.3 m/s^2 [11]
Rotation Period:	3.5 days		
Temperature Range:	n/a		
Atmospheric Pressure:	100 nbar	Composition:	O_2
Surface Material and Morphology:		Smooth ice, dirty geysers	

Table 2.10: Europa surface conditions

NASA's *Jupiter Icy Moon Orbiter*, which is in the early stages of planning, will be designed to circle each Galilean moon for up to a year, to allow detailed investigations of these worlds. This mission is a first step for advanced robotic missions to study the habitable environments of the outer moons in detail.

Ganymede (Jupiter)			
Radius:	2634 km	Gravity:	1.4 m/s^2 [12]
Rotation Period:	7.1 days		
Temperature Range:	117–156 K [12]		
Atmospheric Pressure:	"thin"	Composition:	O_2
Surface Material and Morphology:		Cratered dirty ice	

Table 2.11: Ganymede surface conditions

Callisto (Jupiter)			
Radius:	2409 km	Gravity:	1.2 m/s^2 [13]
Rotation Period:	16.7 days		
Temperature Range:	128–168 K [13]		
Atmospheric Pressure:	n/a	Composition:	n/a
Surface Material and Morphology:		Cratered dirty ice	

Table 2.12: Callisto surface conditions

All other Jovian moons are not qualified for traditional robot exploration because of their small sizes.

Titan is the largest of Saturn's so far confirmed 47 moons and the second largest natural satellite in the solar system. It is the only moon in our solar system to have a dense, fully developed atmosphere that consists of more than just trace gases. In 2005 a first probe *Huygens*, deployed from the *Cassini* orbiter, reached Titan and delivered valuable information regarding mainly its atmosphere. The moon remains a site of high interest for space exploration, as it is believed to contain complex, pre-biotic chemistry. An overview of its characteristics is given in Table 2.13.

Titan (Saturn)			
Radius:	2575 km	Gravity:	1.3 m/s^2
Rotation Period:	15.9 days		
Temperature Range:	71–94 K		
Atmospheric Pressure:	1.44 bar	Composition:	N_2, CH_4
Surface Material and Morphology:		Mostly solid, atmospheric debris	

Table 2.13: Titan surface conditions

Triton is Neptune's largest moon, of its known 13. It has a complex geological history with a relatively young surface and its therefore of interest for exploration. Triton's attributes are referred to in Table 2.14.

All other natural satellites in our solar system are too small for the envisioned type of mission.

Triton (Neptune)			
Radius:	1352 km	Gravity:	0.8 m/s^2
Rotation Period:	n/a		
Mean Temperature:	38 K		
Atmospheric Pressure:	14 μbar	Composition:	N_2, CH_4
Surface Material and Morphology:		Even, icy	

Table 2.14: Triton surface conditions

2.4.3 Comets and Asteroids

A comet is a small body in the solar system that orbits the sun and exhibits a coma (or atmosphere) and/or a tail, both due primarily to the effects of solar radiation upon the comet's nucleus, which itself is composed of rock, dust, and ices. A summary with relevant information is given in Table 2.15.

Comet	
Diameter:	few km
Temperature:	Dependent on solar irradiation
Atmosphere:	Continuously looses gas, dust
Surface Material and Morphology:	Frozen gases, silicate dust

Table 2.15: Comet surface conditions

The small size of comets prevent them from being targets for traditional robot surface exploration missions, as they not even gravitationally contain their own gasses.

An asteroid is a small, solid object in our solar system, orbiting the sun and is an example of a minor planet (or planetoid), which are much smaller than planets. A summary with relevant information is given in Table 2.16.

Asteroid	
Diameter:	200–1000 km and smaller
Temperature:	Dependent on solar irradiation
Atmosphere:	None
Surface Material and Morphology:	Crust of dust and rock

Table 2.16: Asteroid surface conditions

Again, sizes are too small to ensure a controlled robotic operation on the celestial body surface.

2.5 Thermal Control Architecture of Mars Exploration Rovers

To gain a deeper understanding of the challenges faced in space application thermal design paradigms, a detailed analysis of the most recent robot surface exploration mission was conducted, the Mars Exploration Rovers (MER), launched in June and July of 2003. Both rovers have well exceeded their design lifetime by more than a factor of 8 and a robust thermal design of the rovers has contributed significantly to their longevity and science productivity.

2.5.1 Flight Mission Description

The MER spacecraft was designed to take a rover and lander from the Earth to Mars (during the cruise phase), through the Mars atmosphere and onto the surface (during the entry descent and landing phase), where the rover conducts science investigations of the Mars geology (during the surface phase). In order to accomplish these varied functions, the flight system consisted of a a cruise stage, an aeroshell entry vehicle, a tetrahedral lander structure and a rover.

2.5.2 Thermal Design Drivers

Hickey *et al.* (1996, [14]) broke down 5 distinct environments, which the rovers must endure. They are ground operations before and after the integration of the Radioisotope Heater Units (RHU), the cruise stage inside the lander, the first day on Mars when the rover is still attached to the lander and the mission phase of the exploration phase on the Martian surface. These five phases of operation drove the design and characteristics of the Mars rovers.

The thermal design of the rovers was influenced by a number of factors. The primary thermal design drivers identified by Novak *et al.* (2003, [15]) are the Mars external environment, hardware temperature limits, electrical energy usage limitations levied by the power system and high and low energy operational scenarios devised by mission planners.

Mars surface environment The Mars surface thermal environment defines the ultimate thermal sink for the rovers. It is driven by such factors as landing site latitude, time of year, ground characteristics, the amount of dust in the atmosphere and landing site elevation.

Hardware temperature limits Hardware temperature limits play a major role in determining the appropriate rover thermal control design. Items that are highly sensitive to extreme cold Mars nighttime temperatures and to wide temperature swings must be shielded from the Martian environment.

Power system constraints and operational scenarios Rover operational scenarios were defined by mission planners and translated into power profiles. A worst-case hot and cold profile were so determined.

2.5.3 Rover Thermal Design Description

The MER thermal design is described by Novak *et al.* (2005, [16]).

Internal Thermal Design Sensitive electronics which have to be protected from freezing in the Martian environment are housed inside the Warm Electronics Box (WEB). A primary focus of the WEB thermal design is to maximize its thermal time constant, by maximizing the thermal resistance. This is done by means of carbon-opacified silica aerogel insulation and low emissivity surface finishes.

All hardware inside the WEB is protected against under-temperature conditions by survival heaters that are switched on by mechanical thermostats. Two paraffin-actuated heat switches, developed by Pauken *et al.* (2002, [17]), prevent the electronics from overheating by rejecting heat to a pair of radiators on the outside of the rovers.

Non-electrical Radioisotope Heater Units (RHU) are used to help keep the rover electronics module and battery warm at night. The RHUs dissipate approximately 1.0 W apiece and weigh 40 g. A a system level description is provided by Rinehart (2001, [18]).

External Thermal Design The principle hardware items located outside the WEB that require thermal control are the cameras, actuators and bearings, and they are equipped with warmup heaters. All of the rover external hardware can survive in a non-operation condition without any survival heat and thermal insulation.

2.5.4 Analytical Thermal Model

An analytical thermal model of the rover was created to provide rapid thermal evaluations of operational profiles during flight operations. The mission operations model is correlated to data obtained in thermal vacuum testing of the flight vehicles.

One of the critical functions of the flight rover thermal model is to predict how long external mechanisms need to be heated prior to use. 5°C of margin is held in heating estimates and temperature predictions, even though results are often better (Novak *et al.* 2005, [16]).

2.5.5 Operations Flight Experience

The MER thermal design has proven itself to be very robust on the Martian surface. During the hottest times of the mission it allowed full functionality of the rover without overheating. During the coldest times of the mission, the rover was able to function with only a minimal amount of electrical survival heater power. The rover thermal design, by maximizing the thermal time constant for electronics inside the insulated WEB, minimized potentially damaging depths of temperature cycles and the amount of energy needed to accomplish thermal control of the vehicle.

2.5.6 Lessons Learned

Nonetheless, lessons were learned during MER operations.

A passive thermal design should be biased to protect against the cold environment, i.e. minimize heat leaks. Transient hot problems are usually solved with a duration or time-of-day operations constraint on the rover. Transient cold

problems will need to be solved by survival heaters, costing valuable electrical energy that could be used for science.

Testing hardware at qualification temperature limits having significant margin beyond Allowable Flight Temperature (AFT) limits is also extremely important.

On a more general basis, the European Space Agency (ESA) (2004, [19]) released a document listing the lessons learnt and recommendations made for future robotic exploration missions on Mars after the mission failure of the *Beagle 2* lander in 2003. These are however based primarily on organizational and managerial considerations.

Implications for Study

Many aspects and reflections made during the design process of the MER rovers can be adopted in the present study. One must however note, that since a semi-autonomous operating mission is planned, temperature regulation by taking influence on the operation status should be avoided as much as possible.

Chapter 3

Thermal Design Framework

3.1 Requirements on Design

For the successful thermal design of any object, a detailed analysis of requirements must be conducted, taking all aspects into consideration. The harsh space environment and unusual life cycle of space applications lead to very challenging constraints in the design process, which have to be fulfilled at all times to ensure reliable operation. These include in the most general case extreme dimensional stability of the spacecraft and instrument, typically with very tight and stable temperature control, as noted by Swanson and Birur (2003, [20]).

3.1.1 Heat Loss Minimization

Due to the limited amount of fuel on board each exploration robot, it is of utmost importance to limit the external heat loss, e.g. during flight cruise or a possible hibernation state. The available fuel should be used as little as possible for active survival heating purposes since this relates directly to the robot lifespan, which is considerably limited if fuel is used for other than mission specific operations.

3.1.2 Active Thermal Control

To guarantee a smooth and continuous operation of the robots, an active thermal control must be provided to prevent the possibility of overheating. This may occur when the robots are highly insulted to limit external heat loss under prolonged use. The robot body temperature is controlled either by limiting the amount of produced heat through operational adjustments or adapting the heat loss rate. This is achieved by means of a thermal control heat rejection mechanism, which must be operated with as little external energy input as possible.

3.1.3 Thermal Robustness

The thermal design architecture must further be very robust, i.e. only small thermal stresses are allowed. This includes the pursuit of a high thermal insulation and shielding, which limits the effects from external influences, and the minimization of stresses imposed on components resulting from different

material thermal expansion coefficients. First is related to the required tight temperature control and second to the mechanical structure durability.

3.1.4 Mechanical Robustness

In addition to the thermal robustness, the robots must also be mechanically robust. This is necessary to meet structural requirements for spacecraft launch loads and impact landings on celestial bodies. Hickey *et al.* (1996, [14]) report these to be as high as 60 g on Mars for example. No damage to the structure is tolerated in these conditions and will be thoroughly tested in a mission qualification test plan as described by Biter *et al.* (2005, [21]).

3.2 Pursued Approach

Different technologies, established or in development, help meet the requirements stated above and contribute in finding a fundamental design philosophy for the paradigm.

3.2.1 Low Emissivity Coating

Due to the frequent absence of an atmosphere in space applications, radiation, which does not require a propagating medium, is often the major source of heat loss. The only way to limit this is by low emissive surface finishes for external facings, as well as internal components.

Surface coatings reach emissivity values as low as 0.01 (silver), according to Lienhard and Lienhard (2005, [22]), and silver or gold coatings have proven to be very effective in minimizing heat loss in space missions.

3.2.2 Thick Insulation Layer

A high thermal insulation and shielding of an object, to protect it against external temperature swings, is achieved by an effective insulation layer in addition to the low emissivity coating. Besides this thermal robustness, the mechanical robustness can also be controlled by this means if the insulation layer's mechanical properties allow it to do so.

In the event of an atmosphere presence, the insulation layer further limits convective heat losses.

Silica Aerogel

Of all available insulation materials, silica aerogel claims the lowest conductivity. At the same time it possesses the lowest density of any solid ($\rho < 0.1$ g/cm^3) due to porosity rates of over 98%, as reviewed by Akimov (2003, [23]). It is a solid state substance, similar to gel where the liquid component is replaced with gas.

The reason for the extremely low conductivity, which reaches less than 20 mW/(m·K) in air, is due to the fact that the interstitial space between material of the aerogel (whether it be voids, particles or fibers) becomes smaller than the mean free path of the gas. The mechanism for gas transport then shifts from the continuum regime to free molecular conduction in the Knudsen

regime. Effective gas conduction is then dominated by the conductive-radiative component of the silica aerogel structure. Direct conduction is however minimized by the low density of the material (Hickey 1996, [14]). An image showing the structure of silica aerogel is shown in Figure 3.1 (Akimov 2003, [23]).

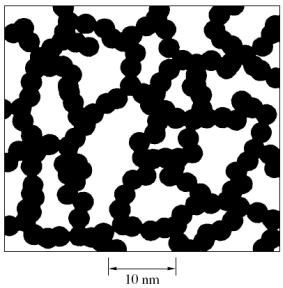

Figure 3.1: Silica aerogel structure

As gas pressure decreases, so does the conductivity of the aerogel, which reaches values of even less than 10 mW/(m·K) in nitrogen vacuum chambers, simulating a space environment. By adding carbon into the silica aerogel structure, to block the infrared component of radiant heat transfer within the aerogel, Lee *et al.* (1995, [24]) were able to further improve the thermal properties. The results are seen in Figure 3.2.

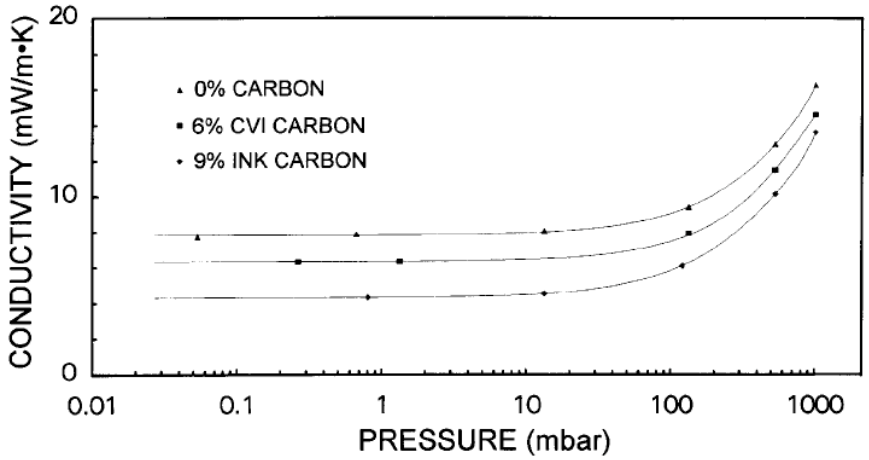

Figure 3.2: Total apparent thermal conductivity of silica aerogel samples against gas pressure at 20°C

Silica aerogel is a very fragile and brittle material, it is however capable to sustain comparably high compressive pressures. As Parmenter *et al.* (1998, [25]) showed, it and can be reinforced by fibers to improve its mechanical properties. Granulated silica aerogel, as investigated by Reim *et al.* (2004, [26]), is also used to pursue identical goals. The fact that silica aerogel is incorporated in the thermal control architecture of the Mars Exploration Rovers shows that it is able to withstand mission qualification testing for purpose of insulation.

3.2.3 Variable Emittance Coating

To control the body temperature of the robots without influencing the fuel cell heat generation, ways must be found to vary their external heat loss. Variable Emittance Coatings (VEC) are one way to influence radiative heat loss according to the exigencies. Two prototypes of this adaptive thermal control system, one based on micro-machined louver technology and the other on electrostatic switches, will be tested on NASA's upcoming *ST-5* spacecraft satellite mission, scheduled for launch early 2006. Other devices of the same purpose make use of electrochromic and electrophoretic technologies.

Micro Electro-Mechanical Switched Radiator

Osiander *et al.* (2004, [27]) devised a Micro Electro-Mechanical System (MEMS) switched radiator. The system consists of MEMS arrays of gold-coated sliding shutters and allow an overall device apparent emittance range of over 40% change when exposing the underlying high emissive silicon. Results are further improved significantly when revising certain prototype specific characteristics. Figure 3.3 illustrates the operating principle of the device.

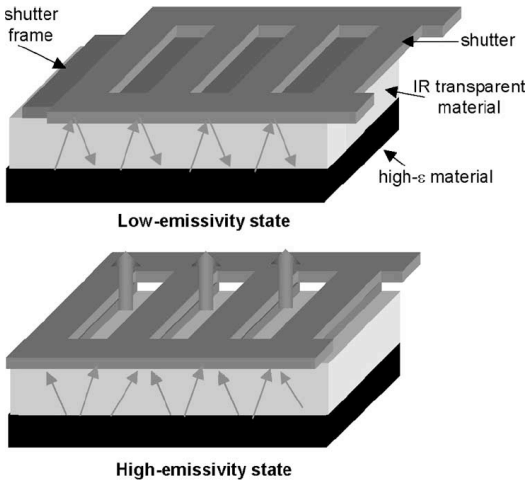

Figure 3.3: Micro Electro-Mechanical switched radiator operating principle

Electrostatic Switched Radiator

An electrostatic switched radiator (ESR) designed by Biter *et al.* (2002, [28]) functions in essence as a thermal switch and changes the mode of heat transfer between the spacecraft skin and radiator film from radiation to conduction, as a cover film is attracted to the spacecraft surface electrostatically. The progress made over several years of development can be witnessed in Biter *et al.* (2004, [29]) as apparent emittance changes of up to 80% were reached. The mode of operation is sketched in Figure 3.4.

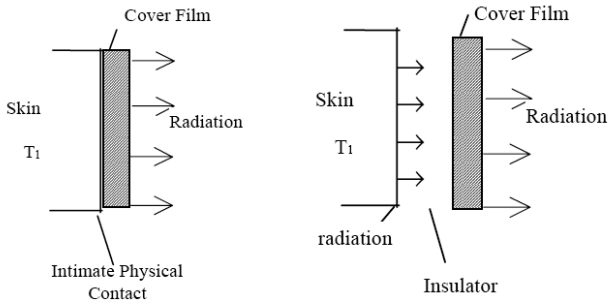

Figure 3.4: Electrostatic switched radiator (ESR) operating principle

Control

Electric control units are responsible for operating the different devices. Farrar *et al.* (2003, [30]) describe the test and evaluation approach for the specific application on the *ST-5* spacecraft mission, yet the information also provides a guideline for future experiments regarding thermal applications on the exterior structure of spacecrafts.

3.2.4 Heat Switch

A further approach to take influence on the interior temperature of the robots is to use a heat switch and conduct heat from the robot inside to the outside shell, shunting the silica aerogel insulation layer. The excess heat is rejected either to the surface of the celestial body or the surrounding atmosphere, which provide the final heat sink. Because of the largely unknown celestial body thermal characteristics, possible large variations between sites and generally low thermal conductivities, interaction with the atmosphere is however favored, as it is much more predictable. The robot shell surface has to be highly conductive in this case, to distribute all heat evenly around.

Desired properties of the thermal switch device are high thermal resistance at rest, high thermal conductance when activated and low power consumption. Additionally the switch must be small and low weight, possibly MEMS embedded. Several approaches exist to meet the requirements.

Paraffin Actuated Switch

A paraffin actuated heat switch was designed for the thermal control of the batteries used in the Mars Exploration Rovers. Above 18°C the paraffin wax inside the switch melts, expands and mechanically closes the switch for heat rejection to a radiator to prevent overheating (Pauken *et al.* 2002, [17]).

Bi-Metal Switch

Milanez and Mantelli (2003, [31]) developed a passively actuated bi-metallic heat switch for space applications in cryogenic systems of satellites. The working principle is based on the differential thermal expansion of distinct metals. An illustration of the device is seen in Figure 3.5.

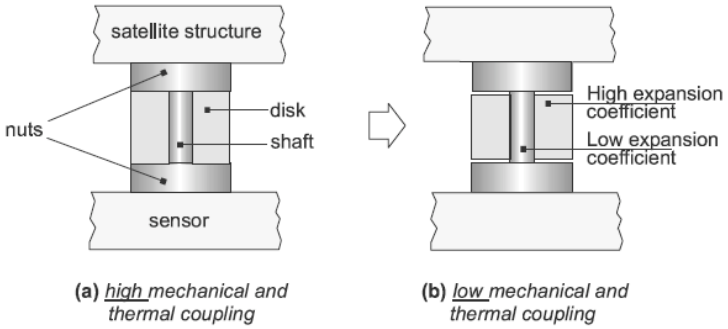

Figure 3.5: Bi-metallic heat switch for space applications

Electrostatic Switch

Similar to the ESR, Slater *et al.* (1996, [32]) devised a switch to control heat flow between two thermally isolated surfaces by bringing the surfaces into intimate mechanical contact, using active electrostatic actuation. The two plates are separated by thermal insulators (polyimide), between 10 and 20 μm thick, to minimize conductive heat transfer.

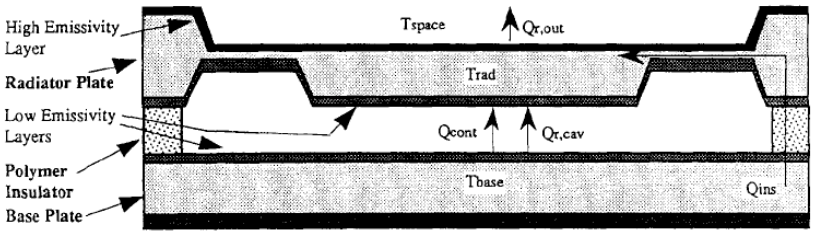

Figure 3.6: Side view of electrostatic switch

3.2.5 Implementation

To this date, no thermal control components exist which could be readily incorporated in the exploration robots to meet specific needs and exigencies. Once the thermal architecture design stage is therefore accomplished, a detailed specification process must be taken up to define the requirements of the necessitated parts which are to be developed. The realization is however most likely to be based on presently emerging technologies, as previously described.

Chapter 4

Thermal Model

4.1 Model Description

Based on all considerations made in Chapter 3, a fundamental thermal control architecture can be devised and incorporated into a model for first heat transfer analyses.

The model consists of a spherical shell, representing the robot shape, with a low outer emissivity coating (ϵ_s) and a thick inner insulation layer (λ_{in}). Further it provides a contact area to the supporting surface and a homogeneous spherical body which contains all components of a single robot. Variable Emittance Coatings on the shell and a heat switch are optional. Figure 4.1 shows a schematic of this configuration.

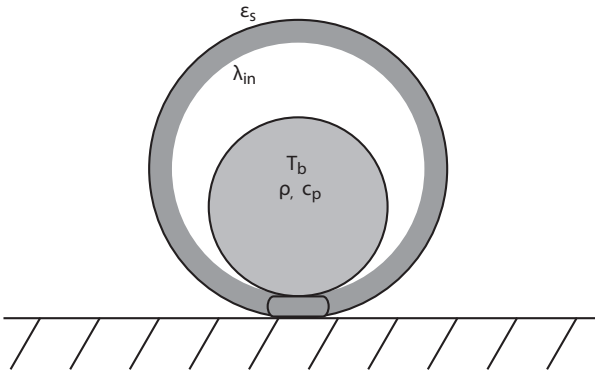

Figure 4.1: Thermal model schematic of exploration robots

Imposed constraints on the dimensions are according to the robot specifications of Plante (2005, [33]) the diameter D and mass m. Table 5.1 in Chapter 5 includes these values. All other design parameters are still influenceable.

This first model will disclose which provisions regarding thermal control have to made in the final design stage of the robots.

4.2 Model Assumptions

For any model to be successful and useful, approximations and assumptions must be made.

Spherical Shapes All shapes in the model, shell and body, are considered to be spherical. Convection correlations are also related to spherical bodies. The aim is to simplify geometric properties, to be able to work with analytical heat transfer equations to reach first approximations in a timely manner.

Isothermal Body The robot body temperature is assumed to be identical in all locations, an assumption which can be made when considering the thick thermal insulation layer which surrounds the body.

Homogeneous Body All properties of the body are considered to be homogeneous. This favors isothermal body conditions.

Uniform Heat Production Internal heat production of the robot fuel cell is taken as uniform, without fluctuating elements, to simplify simulations.

Uniform and Constant Outer Temperature Outer temperatures are regarded as being time independent and identical in any point.

Outer Temperature Equal to Supporting Surface Temperature Due to the robot's small size compared to the planetary or lunar terrain, the supporting surface temperature is the major external temperature influence on the robot heat transfer.

Inner Insulation Surface Temperature at Body Temperature To facilitate modeling, the inner insulation temperature is assumed to be at body temperature. This would represent an upper-bound scenario, where all heat from the body is directly released to the insulation material without additional insulation or shielding from low emissive component surface finishes.

Steady State for Heat Transfer Analyses Heat transfer analyses, to estimate the heat loss of the robots, are all conducted under steady state conditions. Calculations were simplified this way, but results also easier to interpret.

Surface Contact Area Temperature Identical to Outer Temperature This upper limit is used in a first approach. The celestial body however represents a semi-infinite slab in a more accurate heat transfer model and must be taken as such into account when ground losses prove to be significant.

Switch Either "On" or "Off" The heat switch to control heat rejection from the robot body can only be influenced in its state of being conducting or non-conducting. No gradual transition changes are considered.

4.3 Heat Transfer Modes

With the exploration robots being located on the surface of a planet or moon containing an atmosphere, all heat transfer modes play a role in heat exchange. Namely conduction through the insulation layer ($\dot{Q}_{cond,s}$) and into the ground ($\dot{Q}_{cond,g}$), as also radiation ($\dot{Q}_{rad}$) and convection ($\dot{Q}_{conv}$) from the shell surface, as seen in Figure 4.2.

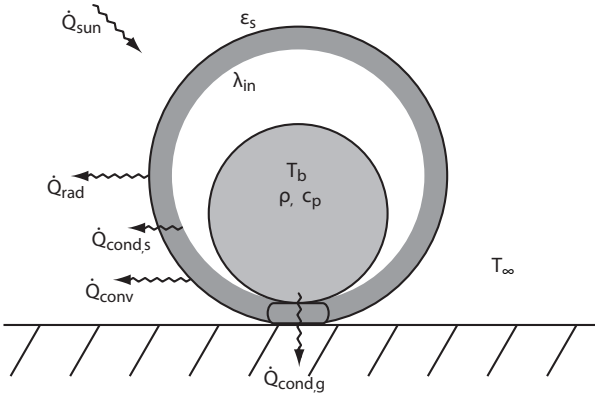

Figure 4.2: Modes of heat transfer involved in robot heat loss

To derive the contribution of the different heat transfer modes to the overall heat loss, they will be broken down below.

4.3.1 Radiation

Heat radiation plays a major role in all space applications due to the frequent absence of an atmosphere. According to Lienhard and Lienhard (2005,[22]) heat radiation of a sphere in a large enclosure is modeled the following way:

$$\dot{Q}_{rad} = \sigma \cdot \mathcal{F}_{s\infty} \cdot A_s \cdot \left(T_s^4 - T_\infty^4\right), \tag{4.1}$$

with the transfer factor $\mathcal{F}_{s\infty}$ approaching the shell surface emissivity ϵ_s

$$\mathcal{F}_{s\infty} \approx \epsilon_s \ , \tag{4.2}$$

because the enclosure area is considered to be much larger than the object area

$$\frac{A_s}{A_\infty} \approx 0 \ . \tag{4.3}$$

σ is the Stefan-Boltzmann constant and equals:

$$\sigma = 5.670 \cdot 10^{-8} \ \frac{\mathrm{W}}{\mathrm{m}^2 \cdot \mathrm{K}^4} \ . \tag{4.4}$$

A_s the shell surface area, A_∞ the enclosure area, T_s the shell surface temperature and T_∞ the surrounding temperature.

Solar Irradiation When knowing the distance from the sun r, a maximum heat flux from incoming solar irradiation can be derived by making use of radiation heat exchange principles, as presented by Modest (2003, [34]):

$$I_{sun} = \sigma \cdot \left(\frac{r_s}{r}\right)^2 \cdot T_{sun}^4 \ , \tag{4.5}$$

where r_s is the radius of the sun

$$r_s = 0.696 \cdot 10^9 \text{ m} \tag{4.6}$$

and T_s the black body temperature of the sun

$$T_{sun} = 5780 \text{ K}. \tag{4.7}$$

When considering, that only half of the robot surface is exposed to incoming solar radiation, the amount of absorbed irradiation by the exploration robots is then after Siegel and Howell (2002, [35]) equal to:

$$\dot{Q}_{sun} = \epsilon_s \cdot \frac{A_s}{2} \cdot I_{sun} \ . \tag{4.8}$$

From Equations 4.5 and 4.8 an equilibrium temperature for gray diffuse bodies solely submitted to solar radiation is determined, if they are merely subject to radiative heat loss:

$$T_{hot} = T_{sun} \cdot \sqrt{\frac{r_s}{r}} \ . \tag{4.9}$$

This value is considered to be the highest achievable temperature on a planet or moon if no internal heating takes place from the core (geothermal gradient) and no atmosphere is present to favor heating by greenhouse effects. No object on such a surface, exposed to solar radiation, can surpass this temperature.

4.3.2 Conduction

Conduction through the insulation layer of the robots is described by solving the conduction equation (Fourier's law) for spherical bodies as shown in Incropera and DeWitt (1996, [36]):

$$\dot{Q}_{cond,s} = \frac{4 \cdot \pi \cdot \lambda_{in} \cdot (T_b - T_s)}{\frac{1}{\left(\frac{D}{2} - x\right)} - \frac{1}{\left(\frac{D}{2}\right)}} \ , \tag{4.10}$$

where λ_{in} is the conductivity of the material, T_b the body temperature and x the insulation layer thickness. The contact area A_{cont} between the robots and the supporting surface is not taken into consideration.

Heat loss into the ground is described in its easiest manner by a one dimensional heat conduction equation (Incropera and DeWitt 1996, [36]):

$$\dot{Q}_{cond,g} = \lambda_{in} \cdot A_{cont} \cdot \frac{T_b - T_\infty}{x} \ . \tag{4.11}$$

If heat loss into the ground though substantially adds to the overall heat loss, the supporting surface must be modeled as a semi-infinite slab and not isothermal, as most celestial bodies are made up of low conductivity surfaces.

4.3.3 Convection

Continuum Requirement In order for convection to play a role in heat transfer, continuum conditions must be satisfied. As Chen (2005, [37]) shows, the Knudsen number is used to verify this:

$$Kn = \frac{l}{D} \ , \tag{4.12}$$

where l is the mean free path of a particle in the surrounding atmospheric gas. If $Kn \ll 1$ continuum conditions are verified.

From kinetic gas theory for an ideal gas, as presented in Kestin and Dorfmann (1971, [38]), the mean free path of a particle is computed as:

$$l = \frac{R \cdot T_\infty}{\sqrt{2} \cdot \pi \cdot d^2 \cdot N_A \cdot p} \ , \tag{4.13}$$

where R is the universal gas constant

$$R = 8.314 \ \frac{\mathrm{J}}{\mathrm{mol} \cdot \mathrm{K}} \tag{4.14}$$

and N_A the Avogadro Number

$$N_A = 6.022 \cdot 10^{23} \ . \tag{4.15}$$

d is the particle diameter and p the atmospheric gas pressure.

Convective Heat Loss Heat convection is determined by the following equation if it plays a role in heat transfer (Incropera and DeWitt 1996, [36]):

$$\dot{Q}_{conv} = h \cdot A_s \cdot (T_s - T_\infty) \ , \tag{4.16}$$

where h is the heat transfer coefficient

$$h = \frac{\lambda \cdot \overline{Nu_D}}{D} \ . \tag{4.17}$$

λ is the thermal conductivity of the surrounding gas which works out for an ideal gas according to Kittel (1980, [39]) to:

$$\lambda = \frac{n \cdot \overline{c} \cdot l \cdot c_v}{3 \cdot N_A} \ , \tag{4.18}$$

with n being the number of particles particles per unit volume in an ideal gas

$$n = \frac{p \cdot N_A}{R \cdot T_\infty} \ , \tag{4.19}$$

$\overline{c}$ the mean particle velocity for a Maxwell-Boltzmann distribution function

$$\overline{c} = \sqrt{\frac{8 \cdot R \cdot T_\infty}{\pi \cdot M}} \tag{4.20}$$

and c_v the specific heat capacity at constant volume

$$c_v = c_p - R \ , \tag{4.21}$$

where c_p, the specific heat capacity at constant pressure, is a function of temperature

$$c_p \sim f(T) \ . \tag{4.22}$$

M is the molar mass of the gas molecules.

For a non ideal gas, the thermal conductivity may however be approximated as a function of temperature and tabulated correlations exist for most common gasses.

Free Convection If there is no wind, free convection is the prevalent form of convective heat transfer and the dimensionless Nusselt number Nu_D, which describes the gas temperature gradient at the solid surface, is described the following way for spherical objects (Incropera and DeWitt 1996, [36]):

$$\overline{Nu_{D,free}} = 2 + \frac{0.589 \cdot Ra_D^{1/4}}{\left[1 + (0.469/Pr)^{9/16}\right]^{4/9}} \ , \tag{4.23}$$

where Ra_D is the Rayleigh number, the product of the Grashof number Gr_D and Prandtl number Pr

$$Ra_D = Gr_D \cdot Pr = \frac{g \cdot \beta \cdot (T_s - T_\infty) \cdot D^3}{\nu \cdot \alpha} \ , \tag{4.24}$$

with g representing the gravitational acceleration, β the expansion coefficient, equal to

$$\beta = \frac{1}{T_\infty} \tag{4.25}$$

and ν being the kinematic viscosity

$$\nu = \frac{\mu}{\rho} \ . \tag{4.26}$$

The dynamic viscosity μ for an ideal gas is (Kittel 1980, [39]):

$$\mu = \frac{1}{3} \cdot \rho \cdot \bar{c} \cdot l \ , \tag{4.27}$$

where ρ is the density of the gas

$$\rho = \frac{p \cdot M}{R \cdot T_\infty} \ . \tag{4.28}$$

For a non ideal gas, the dynamic viscosity may however again be approximated as a function of temperature and tabulated correlations exist for most common gasses.

α is known as the thermal diffusivity and is defined by (Incropera and DeWitt 1996, [36]):

$$\alpha = \frac{\lambda}{\rho \cdot c_p} \ . \tag{4.29}$$

The Prandtl number Pr describes the ratio between momentum and thermal diffusivity (Incropera and DeWitt 1996, [36]).

$$Pr = \frac{\nu}{\alpha} \tag{4.30}$$

It provides a measure of the relative effectiveness of momentum and energy transport by diffusion in the velocity and thermal boundary layers.

The previously mentioned Grashof number Gr_D describes the ratio of buoyancy to viscous forces in the velocity boundary layer. Its role in free convection is much the same as that of the Reynolds number Re_D, which is the ratio of the inertia and viscous forces in the velocity boundary layer, in the subsequent treatment of forced convection.

Forced Convection When wind is present in an atmosphere, an alternate correlation for the Nusselt number Nu_D must be employed, taking wind heat transfer effects into consideration. For spheres this is best quantified by the following equation (Incropera and DeWitt 1996, [36]):

$$\overline{Nu_{D,forced}} = 2 + \left(0.4 \cdot Re_D^{1/2} + 0.06 \cdot Re_D^{2/3}\right) \cdot Pr^{0.4} \cdot \left(\frac{\mu}{\mu_s}\right)^{1/4} \quad , \tag{4.31}$$

where Re_D is the Reynolds number with u as wind speed

$$Re_D = \frac{u \cdot D}{\nu} \tag{4.32}$$

and μ_s the dynamic viscosity of the gas at surface temperature

$$\mu_s = \mu\left(T_s\right) \ . \tag{4.33}$$

4.4 Thermal Control Mechanisms

For a thermal control mechanism design, as introduced in Sections 3.2.3 and 3.2.4, to be effective, it has to be able to release at least as much heat as internally produced at any time of operation, under any circumstances. This infers that some parameter must be influenced to vary the heat loss rate.

This type of active thermal control is therefore only applicable in a specific environment where material properties allow it to do so. The aim is to expand this environment as much as possible, preferably to the entire operation range of the robots.

4.4.1 Variable Emittance Coating Emissivity

In Variable Emittance Coatings the apparent surface emissivity $\epsilon_{s,vec}$ influences the robot radiative heat loss according to Equation 4.34, where A_{vec} is the VEC surface area.

$$\dot{Q}_{rad,vec} = \sigma \cdot \left[\epsilon_s \cdot \left(1 - \frac{A_{vec}}{A_s}\right) + \epsilon_{s,vec} \cdot \frac{A_{vec}}{A_s}\right] \cdot A_s \cdot \left(T_s^4 - T_\infty^4\right) \tag{4.34}$$

Figure 4.3 shows this situation, where an additional heat loss term is added to the model.

A minimum value of apparent emissivity is derived this way for different environments, to ensure that heat loss takes place at the desired rate. If this value surpasses 1 the limits of the control mechanism are reached and not all internally produced heat can be radiated off the surface of the robots. This will ultimately lead to overheating.

Since only the apparent emissivity of a coating is of relevance in steady state heat radiation, the variable emittance coating can make use of a mechanism which solely provides a low and high emissive state. These states are then alternated by an electronic control system to match the desired properties of apparent emissivity.

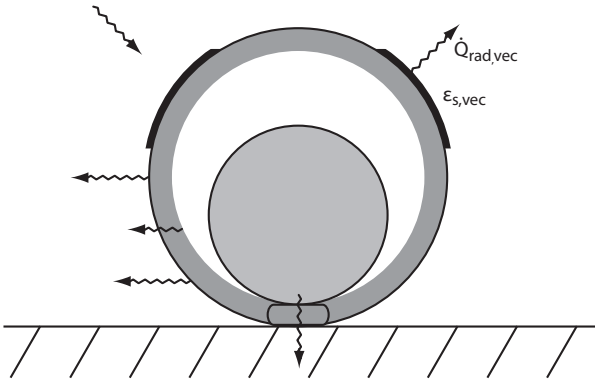

Figure 4.3: Thermal model with Variable Emittance Coating

4.4.2 Switch Conductivity

In the case of the heat switch control device, the parameter of relevance is the thermal conductivity of the switch λ_{sw}, as this limits the maximum heat to be transported through the switch. A one dimensional conduction equation describes this situation in its most fundamental manner, as seen in Equation 4.35, where A_{sw} is the switch contact area and x_{sw} the switch length. Figure 4.4 illustrates the setup on the thermal model.

$$\dot{Q}_{cond,sw} = \lambda_{sw} \cdot A_{sw} \cdot \frac{T_b - T_\infty}{x_{sw}} \tag{4.35}$$

Only if materials are employed which have a thermal conductivity higher than the minimum value prescribed from solving the above equation, enough heat is rejected from the body. Highly conductive materials reach conductivities close to 500 J/(m·K) (Lienhard and Lienhard 2005, [22]).

As a switch only has a binary “on” or “off” state, the overall heat loss must be regulated by a mechanism which opens and closes the switch as required. This is either actively controlled by an electronic control system or passively, for example by a bi-metal or wax switch, as elaborated on in Section 3.2.4.

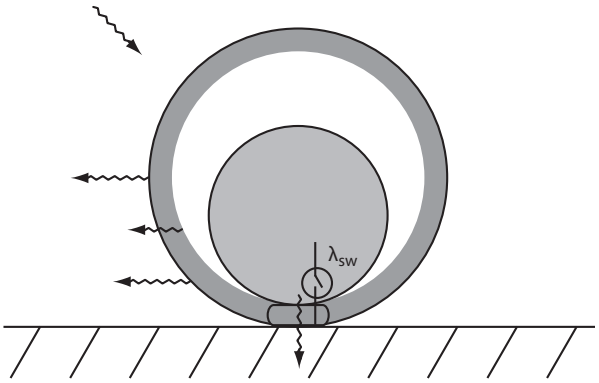

Figure 4.4: Thermal model with heat switch

4.5 Thermoelectric Generator

Because all internally produced heat leaves the exploration robots in one way or another, it is of interest to consider integrating thermoelectric technologies into to the robot design, able to generate electricity from a temperature gradient. The principle of operation for a semiconductor thermocouple is shown in Figure 4.5 (Rowe 1991, [40]).

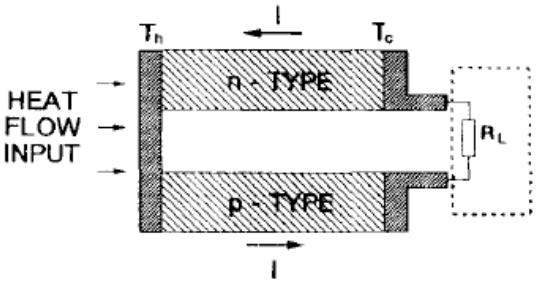

Figure 4.5: Schematic of a semiconductor thermocouple

The overall energy efficiency of the robots increases when a thermoelectric device is installed and the mission duration is consequently prolonged. Figure 4.6 schematically illustrates the system incorporated into the model.

Thermoelectric energy generation, making use of the Seebeck effect, has a long history in spacecraft engineering, especially Radioisotope Thermoelectric Generation (RTG). A technology development review of this field over the past 4 decades was conducted by Rowe (1991, [40]).

The major advantages of the technology are, that it requires no moving parts, making it very reliable, and only very small temperature differences to operate. Conversion efficiencies are however quite low and do not not exceed 10% presently.

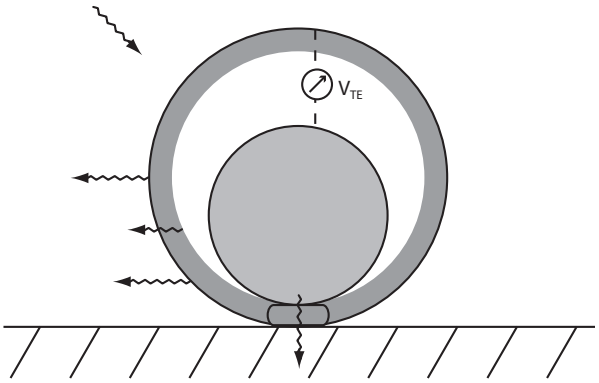

Figure 4.6: Thermal model with thermoelectric heat generator

The theoretical maximum conversion efficiency of a thermoelectric generator according to Rowe (1995, [41]) is:

$$\eta_{te} = \frac{T_b - T_\infty}{T_b} \cdot \left[\frac{M_{te} - 1}{M_{te} + \left(\frac{T_\infty}{T_b}\right)} \right] \quad , \tag{4.36}$$

where M_{te} is equal to

$$M_{te} = \sqrt{1 + Z \cdot \frac{T_b + T_\infty}{2}} \tag{4.37}$$

and Z is the Figure of Merit. The Figure of Merit is a characteristic of a thermoelectric couple, making up the energy producing device, and varies from material to material. Thermocouples based on bismuth telluride possess the highest figure of merit reported and reach values of up to $Z = 3.3 \cdot 10^{-3}$ K^{-1} according to Nolas *et al.* (2001, [42]).

Technical applications however only reach about half of the ideal conversion efficiency values (Rowe 1995, [41]) and would still have to be specifically developed for this particular case.

4.6 Complete Model

Figure 4.7 shows an image of the modeled robots including all heat transfer modes, thermal control provisions and the thermoelectric generator to provide an overview of all aspects considered in the model.

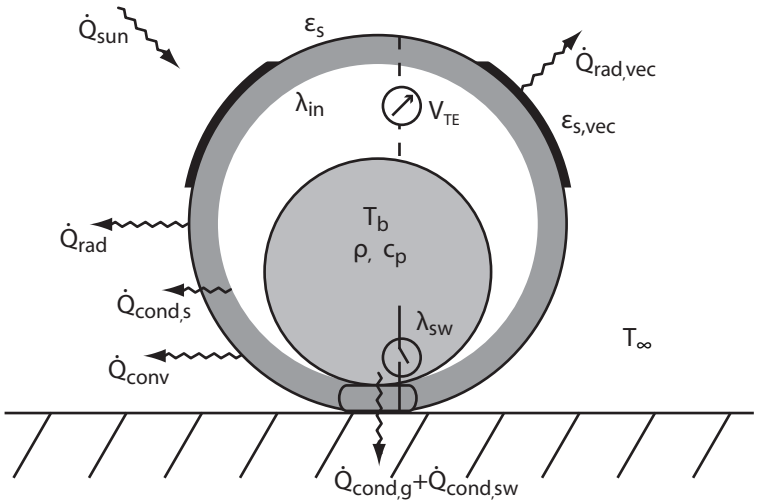

Figure 4.7: Schematic combining all considerations made to thermal model

Chapter 5

Thermal Model Performance Predictions

5.1 Involved Parameters

Table 5.1 regroups all fixed parameters relevant to the robot modeling. They are essential to successful model predictions.

D	=	10 cm	Robot diameter
m	=	100 g	Robot mass
D_b	=	5 cm	Body diameter
T_b	=	300 K	Average body temperature
$(\rho \cdot c_p)_b$	=	$3 \cdot 10^6$ J/(m^3·K)	Body density – specific heat product
x	=	25 mm	Insulation layer thickness
λ_{in}	=	0.005 W/(m·K)	Thermal conductivity of insulation
ϵ_s	=	0.01	Shell surface emissivity
A_{cont}	=	1 cm^2	Robot contact area with surface
$\dot{Q}_{fc}$	=	1 W	Fuel cell energy production
η_{fc}	=	0.65	Fuel cell efficiency
η_{tot}	=	0.02	Heat to mechanical energy efficiency
Z	=	$3.3 \cdot 10^{-3}$ K^{-1}	Thermoelectric Figure of Merit
A_{vec}/A_s	=	0.75	VEC area on shell
x_{sw}	=	3 cm	Heat switch length
A_{sw}	=	1.5 mm^2	Contact area of heat switch

Table 5.1: Fixed robot parameters for thermal simulations

As body diameter, a value was chosen which could realistically fit all components at an appropriate density (1500 g/cm^3). The thermal conductivity of the insulation layer corresponds to the range for silica aerogel in vacuum and the shell emissivity represents a silver coated surface. The Figure of Merit for the thermoelectric device fits numbers for bismuth telluride. Fuel cell relevant information was extracted from the robot specification sheet (Plante 2005, [33]), as the robot diameter and mass. All other values are based on educated guesses.

Mars an Titan are the only celestial bodies, which are being considered as possible mission locations, to contain a notable atmosphere. Their respective atmospheric conditions and other related data is grouped in Tables 5.2 and 5.3. These values are sufficient for first free- and forced convection approximations., when assuming the atmospheric gas to behave like an ideal gas.

g_{mars}	=	3.71 m/s^2	Gravitational acceleration
p_{mars}	=	750 Pa	Atmospheric pressure
u_{mars}	=	2 m/s	Maximum wind velocity
M_{CO_2}	=	44 g/mol	Molar mass of dominant gas component
d_{CO_2}	=	$3.32 \cdot 10^{-10}$ m	Diameter of dominant gas component
c_{p,CO_2}			Heat capacity at constant pressure

Table 5.2: Mars atmospheric conditions

g_{titan}	=	1.35 m/s^2	Gravitational acceleration
p_{titan}	=	144 kPa	Atmospheric pressure
u_{titan}	=	n/a	Maximum wind velocity
M_{N_2}	=	28 g/mol	Molar mass of dominant gas component
d_{N_2}	=	$1.10 \cdot 10^{-10}$ m	Diameter of dominant gas component
c_{p,N_2}			Heat capacity at constant pressure

Table 5.3: Titan atmospheric conditions

Gravitational acceleration and atmospheric pressure values are taken from tables in Chapter 2 describing the various celestial bodies which come into question as mission location. Maximum wind velocities in surface area for Mars are reported in Kaplan (1988, [43]). No data for wind speeds on Titan's surface was found. The gas molecule diameter is derived from the respective bond lengths written down in Lide (2004, [44]). Linear molecules are assumed to be spherical with a diameter equal their length.

Correlations for the temperature dependancy of specific heats at constant pressure are found in Yaws (1999, [45]) and are summarized in Table 5.4 for carbon dioxide and nitrogen. The correlations are valid to a lower limit of 50 K and T_∞ is in Kelvin.

$$
\begin{aligned}
c_{p,CO_2} &= 27.437 + 4.2315 \cdot 10^{-2} \cdot T_\infty - 1.9555 \cdot 10^{-5} \cdot T_\infty^2 \\
&\quad + 3.9968 \cdot 10^{-9} \cdot T_\infty^3 - 2.9872 \cdot 10^{-13} \cdot 10_\infty^4 \ \text{J/(mol·K)} \\
c_{p,N_2} &= 29.342 - 3.5395 \cdot 10^{-3} \cdot T_\infty + 1.0076 \cdot 10^{-5} \cdot T_\infty^2 \\
&\quad - 4.3116 \cdot 10^{-9} \cdot T_\infty^3 + 2.5935 \cdot 10^{-13} \cdot 10_\infty^4 \ \text{J/(mol·K)}
\end{aligned}
$$

Table 5.4: Specific heat at constant pressure temperature correlations

Approximations for an ideal gas were used, because no correlations for the thermal conductivity and dynamic viscosity temperature dependency exist for the gasses in question with a lower limit validity up to 50 K. Due to the small sizes of the gas molecules, approximations for an ideal gas work quite well though

in both cases, as comparisons with experimentally obtained gas characteristics show in coinciding temperature ranges (ca. 200 K) (Yaws 1999, [45]).

5.2 Investigated Parameters

With the developed model, made assumptions and fixed variables, parameters deemed as important and relevant for heat transfer analyses are determined. They are consequently of greatest influence for considerations to be made during the robot design process and are summarized in Table 5.5.

$\dot{Q}_{loss}$	=	$\dot{Q}_{cond,s} + \dot{Q}_{cond,g} \left[+\dot{Q}_{cond,sw}\right]$	[W]
T_s			[K]
η_{inc}	=	$\frac{\eta_{fc}+\eta_{te}/2}{\eta_{fc}} - 1$	[/]
ΔT_b			[K]
$\epsilon_{s,vec}$			[/]
λ_{sw}			[W/(m·K)]

Table 5.5: Investigated parameters in study

Heat Loss $\dot{Q}_{loss}$ describes the overall steady state heat loss from the robot body to its shell and surroundings. It is composed of conduction heat losses through the insulation layer $\dot{Q}_{cond,s}$ and into the celestial body surface $\dot{Q}_{cond,g}$. A component for the thermal control mechanism related heat loss by means of a heat switch ($\dot{Q}_{cond,sw}$) must also be included when incorporated into the model.

Shell Temperature T_s is the robot shell temperature and is an important value to estimate the thermal stress on the robot components and give a first approximation on thermoelectric generation efficiencies.

Efficiency Increase η_{inc} specifies the robot fuel cell efficiency increase in electricity generation if a thermoelectric generator is added. The value is used for lifespan considerations and the correlation is found in Table 5.5. Half of the ideal thermoelectric efficiency η_{te} is used in the equation to simulate technical applications (cf. Section 4.5).

Body Temperature Increase ΔT_b describes the robot body temperature increase during a one hour heating period and is needed for dynamic overheating analyses. This is the only value being computed under transient conditions.

VEC Emissivity $\epsilon_{s,vec}$ represents the minimum value of apparent emissivity a Variable Emittance Coating must possess to be able to reject all internally produced heat from the robot fuel cell.

Switch Conductivity λ_{sw} represents the minimum value of thermal conductivity a heat switch must possess to be able to reject all internally produced heat from the robot fuel cell.

5.3 Physical Relationships

In order to determine the parameters introduced, several additional dependencies and physical relationships must be followed to obtain unique and correct solutions.

For the energy balance of the system to be valid, heat conduction through the insulation layer must equal heat radiated and convected off the robot shell surface. If a VEC is installed, its influence must also be considered in heat radiation. Further, incoming solar radiation ($\dot{Q}_{sun}$) has to be considered when necessary and required. The mathematical formulation is given in Equation 5.1.

$$\dot{Q}_{cond,s} = \dot{Q}_{rad[,vec]} + \dot{Q}_{conv} \left[-\dot{Q}_{sun}\right] \tag{5.1}$$

Equation 5.2 describes the steady state case, where all heat produced by the robot fuel cell is rejected to the exterior. This relationship is fundamental for thermal control considerations, since these mechanisms have to be able to release all internally produced heat.

$$\dot{Q}_{heat,fc} = \dot{Q}_{loss} \tag{5.2}$$

Fuel cell heat production is governed by Equation 5.3. All energy which is not effectively converted into mechanical energy is released as heat. A mission scenario is adopted where one tenth of the electrical power is supplied to the electronic components of the system and the other part to the bistable EPAM actuator mechanism. All factors are already included in η_{tot} and are taken from system level performance calculations (Plante 2005, [33]).

$$\dot{Q}_{heat,fc} = (1 - \eta_{tot}) \cdot \dot{Q}_{fc} \tag{5.3}$$

The robot body temperature increase during heating is inferred from the transient heat transfer equation, as noted in Equation 5.4. All heat non-evacuated from the interior of the robots contributes to a body temperature increase.

$$(\rho \cdot c_p)_b \cdot \frac{4}{3} \cdot \pi \cdot \left(\frac{D_b}{2}\right)^3 \cdot \frac{dT_b}{dt} = \dot{Q}_{heat,fc} - \dot{Q}_{loss} \tag{5.4}$$

5.4 Parametric Study

The results of an undertaken parametric study are presented in the following. The study investigates the average heat loss of the exploration robots in a given environment and determines the requirements thermal control components must fulfill to reject all internally produced heat in the objective to avoid overheating during continuous operation. Further the potential of thermoelectric energy generation is analyzed.

The same identical robot design, with the specified parameters in Section 5.1, is used in each case to produce comparable results for all different situations, in the aim to determine the effects and coherence of varying surroundings on the robots. They consist namely of celestial bodies without a notable atmosphere one the one side and two separately treated environments for Mars and Titan. Both are enclosed by an atmosphere and convective heat transfer phenomena

is included in the respective calculations, as the two atmospheres contribute to the continuum regime of heat transfer effects.

The primary goals of the study are to ensure that freezing and overheating of the robots is prevented. First is the case if the average heat loss does not exceed internally produced heat and second if provisions in the design enable the average heat loss to equal the dissipated heat when needed. Equation 5.5 illustrates the requirements analytically.

$$\dot{Q}_{loss} \leqslant \dot{Q}_{heat,fc} = 0.98 \text{ W} \tag{5.5}$$

The intention of the study is to obtain first order approximations and determine the feasibility of the concept. In a later stage, more elaborate heat transfer models are employed to ameliorate results, especially once the interior robot components are clearly defined.

All calculations were conducted with help of a *Mathematica* code, who's source file is found in appendix A.3.

5.4.1 Passive-Cold Scenario

A so-called passive-cold scenario simulates the robot maximum heat loss under a given outer temperature T_∞ and constant body temperature T_b. These values are vital for freezing and minimal lifespan considerations.

The robot body temperature is kept constant at $T_b = 300$ K during the simulation and no additional heat is produced by the fuel cell to ensure steady state conditions. This represents a minimum robot hopping rate, or a possible hibernation or inoperative state in the exploration mission. In this case no energy is used for mobility purposes and all generated power is dissipated into heat ($\dot{Q}_{heat,fc} = \dot{Q}_{fc}$). Further, incoming solar irradiation is not taken into account, simulating a cave or night time environment.

Results of this analysis include the maximum robot heat loss $\dot{Q}_{loss}$ in a passive-cold case situation, the corresponding shell surface temperature T_s, important for thermal stress considerations, and the robot fuel cell efficiency increase η_{inc} if a thermoelectric generator is added to the setup.

The goal is to ensure as little as possible overall heat loss to increase the robot lifetime and inhibit freezing of components that can not be heated up anymore.

Celestial Bodies without Atmosphere

In a first approach, only conditions are considered where no convection takes place. This is true for all planets and natural satellites looked at as possible mission locations, except Mars and Titan, as they are not surrounded by a dense atmosphere.

Overall heat losses, governed by radiation, are comparably small in this scenario due to the low emissive shell surface finishes. The determined shell temperature is fairly close to the body temperature, which has a limiting effect on the thermoelectric efficiency as is seen in Table 5.6.

The reason for this observation is related to radiation governing heat transfer effects. As this equals conduction through the insulation layer, the temperature difference between insulation boundaries adapts to the required value, which in this case of low overall heat loss is very limited.

T_∞ [K]	$\dot{Q}_{loss}$ [W]	T_s [K]	η_{inc} [/]
50	0.10	270	1.23%
100	0.10	270	1.22%
150	0.09	272	1.15%
200	0.08	276	0.98%
250	0.05	285	0.62%

Table 5.6: Passive-cold scenario for celestial bodies without notable atmosphere

Mars

On Mars, a planet of highest interest for robotic surface and subsurface exploration, both free and natural convection have to be taken into account in the simulation. First simulates a cave situation and second robots located on an open surface exposed to wind. Only the Martian temperature range of roughly 100–300 K is considered for the simulation.

	Free Convection			Forced Convection		
T_∞ [K]	$\dot{Q}_{loss}$ [W]	T_s [K]	η_{inc} [/]	$\dot{Q}_{loss}$ [W]	T_s [K]	η_{inc} [/]
100	0.52	135	6.94%	0.62	105	8.27%
150	0.39	177	5.12%	0.46	154	6.13%
200	0.26	218	3.39%	0.31	203	4.04%
250	0.13	259	1.68%	0.15	251	2.00%

Table 5.7: Passive-cold scenario for Mars

Heat loss values collected in Table 5.7 are significantly higher in both conditions compared to the previous analysis, as the governing external heat transfer component is now convection. It is however limited by conduction through the silica aerogel insulation layer, which confines convective heat loss due to a substantial decrease in shell surface temperature. With the shell temperature dropping, the efficiency increase from thermoelectric energy generation on the other side rises.

Forced convection losses are as expected higher than natural or free convection losses.

Titan

No near surface wind data is available for Saturn's moon Titan, the only known moon to contain an atmosphere. Therefore only free convection is simulated on the model. Its remote distance from Earth makes observations of this type much more challenging than on Mars. The corresponding free convection results are found in Table 5.8 for Titan's temperature range of about 50–150 K.

The data set is analogous to the Mars case for identical reasons. Only absolute heat loss values are higher due to differing atmospheric compositions, mainly pressure and composition elements. Robot shell surface temperatures are consequently slightly lower, implying thermoelectric efficiency increases on the other side.

	Free Convection		
T_∞ [K]	$\dot{Q}_{loss}$ [W]	T_s [K]	η_{inc} [/]
50	0.78	53	10.62%
100	0.62	103	8.38%
150	0.47	152	6.20%

Table 5.8: Passive-cold scenario for Titan

5.4.2 Active-Hot Scenario

A so-called active-hot scenario simulates the robot minimum heat loss under a given outer temperature T_∞ and continuous operation. As this does not necessarily compensate for internal heat production, a thermal control mechanism must adapt the heat transfer rate, so overheating is avoided.

In a first step the transient temperature increase of the robot body ΔT_b during a one hour period is determined, if the fuel cell is operating continuously under full capacity ($\dot{Q}_{fc} = 1$ W) and no thermal control provision is installed to reject excess heat. An impression on the required reaction speed of the thermal control system is gained that way. The initial temperature of the body is $T_b =$ 300 K.

In a second step the demands on the thermal control system are specified, namely the minimum conductivity of the heat switch λ_{sw} and the minimum emissivity value of the Variable Emittance Coating $\epsilon_{s,vec}$, to ensure that no net energy exchange takes place between the robots and their surroundings. All heat rejected by the heat switch is bridged through the silica aerogel insulation layer onto the robot shell, as described in Section 3.2.4. For all Variable Emittance Coating considerations, the shell surface temperature therefore equals the robot body temperature of $T_s = T_b = 300$ K. In the occurrence of an atmosphere presence, heat convection must also be considered at the increased rate when the robot surface temperature equals its body temperature.

The aim is to reach this result of no net heat exchange described in Equation 5.2 with an emissivity of less than 1 for the Variable Emittance Coating and a thermal conductivity of less than 500 W/(m·K) for the switch. First corresponds to a physical boundary and second to the highest material thermal conductivity value known, silver (Lienhard and Lienhard 2005, [22]).

Temperature Relationships with Atmosphere Absence

The effects of an active-hot scenario on body temperature and thermal control system requirements are first identified in conditions laking an atmosphere and not submitted to incoming solar radiation, such as a cave. They are presented in Table 5.9.

The resulting body temperature increase, when heat is accumulated in the robot, is quite low due to the high robot thermal mass with respect to the fuel cell heat production. Heat rejection by means of a coupled heat switch and VEC is extremely effective, as is seen by the very low required surface emissivity values to allow all heat to be radiated off the robots. This is because of the large temperature difference between the surroundings and the robot shell at body temperature.

		Thermal Control	
T_∞ [K]	ΔT_b [K]	λ_{sw} [W/(m·K)]	$\epsilon_{s,vec}$ [/]
50	16	47	0.09
100	16	59	0.09
150	16	79	0.09
200	16	120	0.11
250	17	248	0.17

Table 5.9: Active-hot scenario for celestial bodies without notable atmosphere and solar irradiation

Conditions on Celestial Bodies

In order to consider incoming solar irradiation on a celestial body in the simulation, the distance from the sun must be known. For all considered mission locations this is noted in the tables of Section 2.4. In Table 5.10 the respective values of maximum equilibrium temperature T_{hot} resulting from incoming solar irradiation I_{sun} are summarized for these planets and moons.

The body temperature increase under the described conditions with solar irradiation then follows with the requirements of the thermal control system. For Mars and Titan atmosphere presence is taken into account and the corresponding natural convection heat loss $\dot{Q}_{conv}$ is added for when the heat switch is closed and the shell surface temperature equals body temperature.

			Thermal Control		
	T_{hot} [K]	ΔT_b [K]	λ_{sw} [W/(m·K)]	$\epsilon_{s,vec}$ [/]	$\dot{Q}_{conv}$ [W]
Mercury	634	59	/	/	/
Moon	394	25	/	/	/
Mars	319	20	/	/	/
Gal. M.	173	16	95	0.10	/
Titan	128	8	35	n/a	88
Triton	72	16	52	0.09	/
Pluto	63	16	50	0.09	/

Table 5.10: Active-hot scenario for celestial bodies with solar irradiation and convective heat loss when applicable

On Mercury, the Moon and Mars the maximum equilibrium temperature is above the average body temperature, so no cooling can take place by means of a passive thermal control mechanism. By deploying the robots though on the poles of Mercury, this issue is circumvented as temperatures there do not exceed 135 K. On the Moon, the long rotation period of the natural satellite allows mission scenarios to be solely conducted during a specific time of day, in order to avoid maximum insolation. Missions on latitudes more distant to the equator also avoid the issue.

The comparably low maximum temperature on Mars does not present a drawback in mission planning, as it can easily be incorporated in the robot Allowable Flight Temperature (AFT) limits.

The Galilean Moons, Triton and Pluto compare very much to the previously

treated situation in Table 5.9, as solar irradiation does not play a major role in heat transfer because of their remote distance from the sun.

On Titan natural convection governs the robot heat loss once the heat switch bridges excess heat to the shell surface and increases its temperature to body values. Therefore no maximum emissivity values for the Variable Emittance Coating are reported. The high rate of convective heat transfer only proves the effectiveness of the system. Once all necessary heat is rejected, the switch opens and convective heat loss values drop back to rates determined in Titan's passive-cold case situation (cf. Table 5.8). The notable reduction in body temperature increase, compared to the other planets and moons, is also related to convective heat transfer effects, as it increases overall heat loss.

In general solar insolation does not have a significant influence on the robot body temperature increase, due to the low emissivity surface finishes of the robot shell.

5.5 Model Observations and Conclusions

Primary results of the previously made parametric study are that robot freezing is avoided in all environments and that overheating is efficiently prevented by the designed thermal control mechanism under all circumstances.

Beyond this, additional observations and conclusions are summarized in the following.

Limited Convective Heat Loss When convective heat losses are present in the system, they account for the majority of the heat loss. The effects of convection are however alleviated by the silica aerogel insulation layer which covers the inner side of the robot shell. Due to the coupled heat transfer, the robot surface temperature is reduced by the conductive heat loss, which approaches surrounding temperatures. Radiation only plays a marginal role in this situation and convective heat transfer is limited due to a small temperature difference between the surroundings and robot surface.

This setup allows the exploration robots to be employed in Martian and Titan environments, restricting overall heat loss below the actual heat generation rate, as is seen in Tables 5.7 and 5.8.

Limited Radiative Heat Loss Analogous to the way the silica aerogel insulation layer limits convective heat loss, the same is the case for radiative heat loss in the event where surface emissivity values may be increased by dust or other deposits on the exploration robots.

This underlines the robustness of the thermal control architecture and shows the silica aerogel insulation layer importance in assuring this reliability.

Inefficient Thermoelectric Energy Generation Efficiencies of thermoelectric power generation are based upon the temperature difference between the robot body and shell surface. Even when considering the shell surface temperature to approach surrounding temperatures in environments where convection takes place, the fuel cell efficiency increase in this situation does not exceed 10%. If radiation governs the external heat loss, shell temperatures are much closer to body temperatures and efficiency increases do not exceed 2%.

This limited efficiency increase therefore probably does not value the extra complexity of installing such a system.

Substantial Thermal Stress In the event of convection presence, when the shell temperature drops close to ambient temperatures, thermal stress becomes an issue as temperature differences of over 200 K may be occur between the robot shell and its body. This must be taken during the robot design phase into account.

On planets or moons without an atmosphere, this is not as much of a concern as temperature differences within the robot are smaller.

Coupled Heat Switch and VEC Only when both thermal control mechanisms, the heat switch to bridge excess heat through the insulation layer and the Variable Emissive Coating to radiate it off, are switched in series, an effective thermal control for the exploration robots is provided and heat rejection assured.

Elsewise, without the heat switch presence, the robot surface temperature is not sufficiently increasable to ensure required heat transfer rates due to the silica aerogel insulation layer. Because of the largely unknown celestial body surface characteristics it is also not recommended to rely on the planet or moon as ultimate heat sink, as they are often made up of low conductive, unpredictable regolith soil.

Unnecessary VEC on Titan Titan is the only mission destination where a Variable Emittance Coating can be omitted in the robot design, as free convection governs heat exchange from the robot shell surface. Once the heat switch is closed, the conducted heat is immediately convected off the robot surface, as the high convection values show in Table 5.10, and radiation is negligible in this case.

Upon opening the switch, shell surface temperatures drop back to the passive-cold scenario, thus limiting heat losses.

Necessary VEC on Mars On Mars, as exterior temperatures approach body temperatures in warmer surroundings, convection alone is not able to remove all waste heat and needs to be supported by an increased radiation rate, adjusted by Variable Emittance Coating, to prevent component overheating, as is seen in Table 5.11.

		Thermal Control		
T_∞ [K]	ΔT_b [K]	λ_{sw} [W/(m·K)]	$\epsilon_{s,vec}$ [/]	$\dot{Q}_{conv}$ [W]
225	14	140	n/a	1.3
250	15	227	0.03	0.8
275	17	488	0.19	0.4

Table 5.11: Active-hot scenario for Mars without solar irradiation

Below a critical value, the same situation as on Titan occurs and radiation is not required to support natural convection for heat loss control.

High Emittance Surface Area In the aim to reduce complexity of the overall system, one can envision to provide a highly emissive area on the robot shell instead of the Variable Emittance Coating. It would be connected to the heat switch and able to substantially vary radiation rates, depending on its temperature.

If the switch is open, radiative heat loss is limited due to the low temperature of the high emittance area, approaching surrounding temperatures, because it is insulated by the silica aerogel layer. If the switch is closed, the temperature of the area in question rises to body values, thus increasing heat transfer. An apparent emissivity is so deducted, which has to match values determined in Tables 5.9 and 5.10 to satisfy thermal control demands.

Rudimental Heat Switch Model The heat switch is described analytically by a very simple first order model. Many options exist on how to influence conductive heat transfer through the switch, predominantly by contact area, switch mechanism design and choice of materials.

The presented values merely show the feasibility of the concept and give an impression on the loads to be handled.

Low Internal Temperature Rises The comparatively weak heat source of the robots, with respect to their thermal mass, induces a small temperature rise during the course of an hourlong continuous operation. This allows the thermal control system time to adapt to the new environment and so decreases the risk of overheating.

The critical thermal control reaction time is herewith long enough to allow maintainable time constants.

Negligible Heat Conduction Into Ground Due to the small contact area between the exploration robots and their supporting surface, simulations have shown that conductive heat loss into the ground, when considered isothermal, is very restricted.

This justifies the isothermal approximation in a first approach and the celestial body surface must not be modeled as semi-infinite slab, as additional accuracy is not required at this point.

Upper-bound Conductive Heat Loss In the undertaken study an upper-bound conduction through the silica aerogel layer is examined because the interior surface temperature is set to body values. This can however be notably reduced when providing the robot components with low emissive surface finishes and limiting fixture contacts. An additional shield comparable to a thermos bottle is hereby created.

During the final design phase, this should definitely be the pursued approach when adding and attaching components to the robot interior.

Single Design For All Missions With the proposed thermal design, essentially one uniform structure can be used to be deployed on every considered mission location.

Parallel missions, reducing development costs and increasing collected science data, could thus be conducted.

Chapter 6

Reference Mission Description

6.1 Validity of Results

Even though very simplified models were used to simulate heat transfer on the exploration robots, such as spherical approximations for the robots and their components, ideal gas assumptions for atmospheric environments, convection correlations for spherical bodies and rudimental thermal control models, the results can still be claimed to be valuable for a first design phase. It is important to know the order of magnitude of the numbers one is dealing with, to determine the feasibility of a concept. After this is ensured more detailed analyses can take place, such as Finite Element Modeling (FEM) studies, once all internal components are exactly known.

As the present study is deemed as feasibility study of the project, the obtained results are considered valid for current needs. Obviously the numbers may vary throughout the design and construction phases, the order of magnitude should however be preserved.

6.2 Implications for Possible Mission Locations

The acquired results allow for a more detailed examination of possible mission locations. The requirements for the operation environment inside the robots are that temperatures may not exceed or fall below Allowable Flight Temperatures (AFT) of the robot components, to avoid overheating and freezing. First is inferred from the Tables in Section 2.4 and second from results in Chapter 5. The general condition is given in Equation 6.1.

$$0 < \dot{Q}_{loss} \leqslant \dot{Q}_{heat,fc} \tag{6.1}$$

It is however clear that for all designated mission locations detailed surface environment information is required prior to the deployment of any robots. Exact information on surface near temperature ranges and atmospherical conditions (wind and pressure) with respect to landing site latitude, time of year and

day, and landing site elevation must be known, in addition to ground characteristics, such as conductivity and morphology. This data can only be collected by means of an orbiter mission, launched before the actual in situ surface exploration mission.

From this information individual design requirements for the exploration robots are deducted with respect to their mission site. The design takes the corresponding hot and cold environment limits into account to deduce an architecture which satisfies the needs of low heat loss and effective active thermal control. By sticking with the structure introduced in Chapter 3 thermal and mechanical robustness are further ensured in the design.

6.3 Implications for Possible Mission Scenarios

With a given average mission heat loss $\dot{Q}_{loss,av}$ different operation scenarios can be envisioned for the exploration robots, depending on the mechanism of internal temperature adjustment.

Temperature Adjustment by Hopping Rate A first possible way to adjust the body temperature of the robots is by setting the hopping rate equal to the required internal heat generation to keep the robots warm. In this case, a ratio γ is determined which describes the inoperative passive cooling state to the operative hopping and subsequently heating state. It is defined in Equation 6.2.

$$\gamma = \frac{\dot{Q}_{heat,fc}}{\dot{Q}_{loss,av}} \tag{6.2}$$

Temperature Adjustment by Thermal Control Provision Rejecting heat by the means of a thermal control mechanism, brings much more flexibility to the robot activity, as no considerations during operations regarding overheating have to be made. Due to the same amount of fuel on board though as in the previous case, a decrease in mission duration χ is observed, when all available energy is employed at once. This is described by Equation 6.3.

$$\chi = \left(1 - \frac{\dot{Q}_{loss,av}}{\dot{Q}_{heat,fc}}\right) \cdot 100 \tag{6.3}$$

Maximum Allowable Heating Time A further noteworthy value is the time required to heat the robot body temperature from its minimal Allowable Flight Temperature, to its maximal AFT at a constant average heat loss without additional heat rejection. This value t_{max} is of relevance for transient considerations, but also to determine the required reaction speed of thermal control mechanisms. The differential equation governing the phenomena is given in Equation 6.4 along with the boundary conditions in Equations 6.5 and 6.6.

$$(\rho \cdot c_p)_b \cdot \frac{4}{3} \cdot \pi \cdot \left(\frac{D_b}{2}\right)^3 \cdot \frac{dT_b}{dt} = \dot{Q}_{heat,fc} - \dot{Q}_{loss,av} \tag{6.4}$$

Allowable Flight Temperatures are taken from the robot specification sheet (Plante 2005, [33]).

$$T_b\ (t = 0) = T_{b,AFTmin} = -40°\text{C} \tag{6.5}$$

$$T_b\ (t = t_{max}) = T_{b,AFTmax} = 40°\text{C} \tag{6.6}$$

Table 6.1 lists the previously introduced values for different average heat losses. These numbers allow a first impression on the mission scenario influence of different environments on the exploration robots.

$\dot{Q}_{loss,av}$ [W]	γ [/]	χ [/]	t_{max} [h]
0.05	19.6	94.9%	4.7
0.1	9.8	90.0%	5.0
0.2	4.9	79.6%	5.6
0.3	3.3	69.4%	6.4
0.4	2.5	59.2%	7.5
0.5	2.0	49.0%	9.1
0.6	1.6	38.8%	11.5
0.7	1.4	28.6%	15.6
0.8	1.2	18.4%	24.4

Table 6.1: Mission scenario influence for varying average heat losses

6.4 Mission Profile

The prognosticated mechanical energy released per robot hop is 0.6 J (Plante 2005, [33]). When considering the overall efficiency of the system $\eta_{tot} = 0.02$, a total energy of $E_{jump} = 30$ J must be provided by the fuel to allow the robot to hop at the requested intensity.

The bistable EPAM mechanism (presented in Chapter 2) enables the actuator to be gradually charged and release the stored energy almost instantaneously at the moment of desire. With a fuel cell energy production of $\dot{Q}_{fc} = 1$ W it takes 30 seconds to charge the bistable actuator. This is considered to be the maximum hopping rate of the robots and the graph of this function is seen in Figure 6.1 for an exemplary overall average heat loss rate of $\dot{Q}_{loss,av} = 0.2$ W.

In this case a thermal control provision must however be present in the system to reject excess heat and avoid overheating. Slower hopping rates can also be thought of which require a regulated heat control. This is represented by the red shaded area in the graph. Decreased hopping rates enable a longer mission duration, as the generated power is used for internal heating purposes and not entirely rejected.

If passive cooling of the robots is considered, without making use of a thermal control mechanism, the fastest hopping rate to avoid overheating is much slower. It is represented by the dotted line in the graph. γ visualizes the ratio between both cases and is determined by Equation 6.2. χ illustrates the reduced mission duration between both extreme cases for the same amount of fuel on board. Below the dotted line, no thermal control mechanism is necessary to ensure safe and reliable operation of the robots.

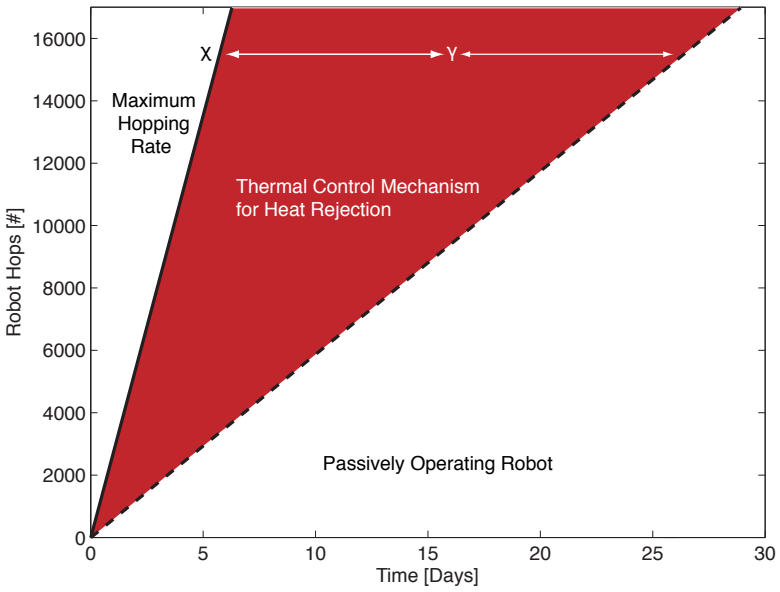

Figure 6.1: Hopping rates mission profile for $\dot{Q}_{loss,av} = 0.2$ W

From Figure 6.1 it is observed, that a heat rejection system has a large influence on the robot mission profile. This allows a very time flexible robot deployment, without loosing any of the envisioned hops or science data. The influence of varying average heat losses on the robot mission scenario can be extracted from Table 6.1. If this mission flexibility however values the additional system complexity, cost and weight of a thermal control mechanism for heat rejection, must be evaluated in a separate study.

Almost identical mission results are obtained if the robots are passively operated and do not rely on a thermal control provision. A silver coated shell with a silica aerogel insulation layer would prevent the robots from freezing and by adjusting the locomotion speed overheating issues are avoided. Only mission deployment flexibility would be slightly compromised as mobility velocity is restricted in the dynamically envisioned semi-autonomous mission scenarios.

6.5 Mission Duration Considerations

The first specification phase of the exploration robots envisions them to carry 30 g of net fuel to power their fuel cells (Plante 2005, [33]). This corresponds to about one third of the robot total mass.

The water producing chemical reaction which takes place in the fuel cell is shown in Equation 6.7.

$$H_2 + 0.5 \cdot O_2 \rightarrow H_2O \tag{6.7}$$

From the $2:1$ hydrogen oxygen mixture ratio and by taking the respective molecular masses into account ($M_{H_2} = 2$ g/mol and $M_{O_2} = 32$ g/mol), the

required hydrogen mass $m_{H_2} = 3.3$ g and oxygen mass $m_{O_2} = 27.7$ g for the robots are determined.

Based on the hydrogen higher heating value ($HHV_{H_2} = 142$ MJ/kg) a maximum robot mission duration for a given average heat loss is derived by Equation 6.8, depending on how much heat it takes to keep the robots warm.

$$t_{mission} = \frac{HHV_{H_2} \cdot m_{H_2}}{Q_{loss,av}} \tag{6.8}$$

Table 6.2 illustrates the maximum mission duration for different average heat losses with a fixed amount of fuel.

$\dot{Q}_{loss,av}$ [W]	$t_{mission}$ [days]
0.05	104.2
0.1	52.1
0.2	26.0
0.3	17.4
0.4	13.0
0.5	10.4
0.6	8.7
0.7	7.4
0.8	6.5

Table 6.2: Mission duration for different average heat losses with 30 g of fuel on board

Equation 6.9 allows the maximum number of jumps for a given mass of fuel to be determined.

$$Max_{hops} = \frac{HHV_{H_2} \cdot m_{H_2}}{E_{jump}} \approx 15\dot{}000 \tag{6.9}$$

This value naturally depends on exactly how much energy is required for the robot's electrical components, a number which should though remain limited in comparison to the required energy for hopping locomotion.

6.6 Mars Deployment Study

In the following, a so-called warm Mars mission scenario, where average mission temperatures are slightly above Martian mean temperatures of 210 K, is considered. This corresponds a situation with an average heat loss of $\dot{Q}_{loss,av} = 0.2$ W. The high thermal mass, effective shielding and high thermal insulation of the robots allow to neglect transient external temperature and internal fuel cell heat generation changes, and solely take the mission average into consideration.

Figure 6.2 shows the situation where a fixed amount of fuel is assumed to be carried by the robots and consequently only a limited number of hops is available. For this particular case the fuel mass is 30 g, which corresponds to 15˙000 hops, as derived in Section 6.5.

As the hopping rates continue to decline, more and more energy is required for active heating, so the robots do not freeze. This denies the system to make

use of all of its energy for hopping and to keep the robot operable, less hops are performed. The blue shaded area represents this effect of active heating.

A maximum mission duration is reached when all energy carried along is required for heating purposes, and is defined by Equation 6.8.

The sharp decline in the active heating slope is explained through the fact that the majority of the internally produced energy is converted to heat, due to the very low overall efficiency. Only very little of the fuel cell generated electricity is not dissipated in the long run.

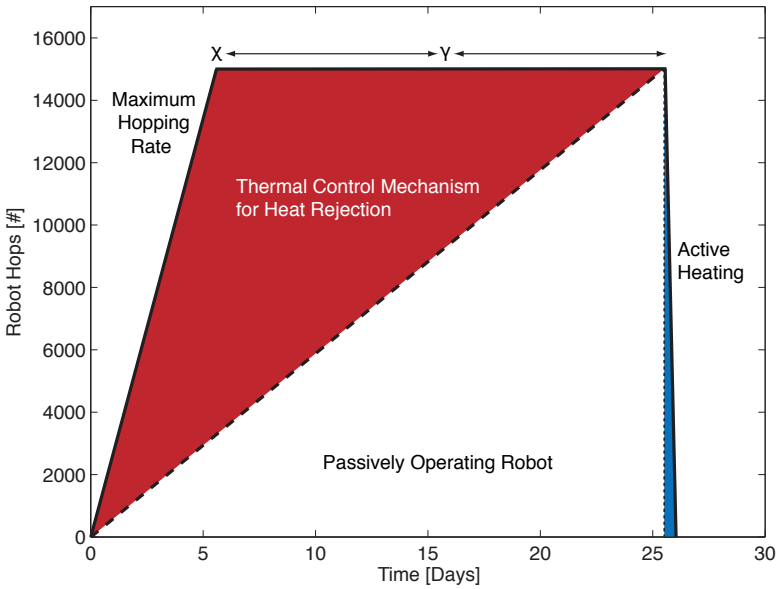

Figure 6.2: Warm Mars reference mission profile with $\dot{Q}_{loss,av} = 0.2$ W and 30 g of fuel on board

6.7 Lifespan Increase by Radioisotope Heating

The scientific, engineering and economic issues at stake for reducing or extending a complex system's design lifetime must be examined from an operator's and manufacturer's perspective, as elaborated by Saleh *et al.* (2006, [46]). A detailed reference mission has to be defined, taking all aspects into consideration, from development demands to the required manpower which has to run operations, in order to evaluate the optimal design lifetime. Lifetime has a significant impact on the overall cost of the spacecraft and mission.

There exists one option though which increases the robot lifespan almost indefinitely if desired. The use of Radioisotope Heating Units (RHU) compensates the constant robot heat loss and fuel cell heat is no longer required for heating. With this system lifetime is extended without altering the amount of energy on board necessary for mobility and science data gathering purposes. These tasks can consequently be covered over a much longer period of time.

Figure 6.3 shows a schematic of a Light Weight Radioisotope Heating Unit (LWRHU) as it is used in the MERs to reduce its overall mass, as it lowers

the required battery energy for heating means. The dimensions reported by Rinehart (2001, [18]) are a length of 3.2 cm, diameter of 2.6 cm and mass of 40 g. 2.67 g of $^{238}PuO_2$ fuel, with a half-life of 88 years, provide a constant heat source of 1 W during the course of the mission.

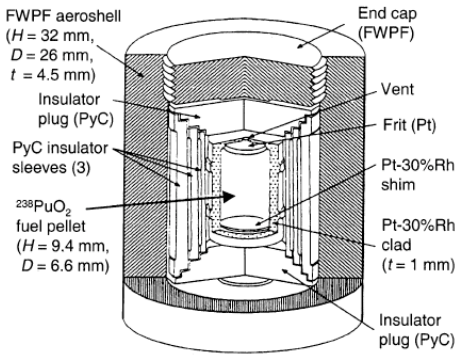

Figure 6.3: Light Weight Radioisotope Heating Unit (LWRHU)

The use of new generation Coated Particles Fuel Compact (CPFC) instead of traditional fuel pellets offer performance increases in the thermal power of RHUs by a factor of 2.3–2.4 and are investigated by El-Genk and Tournier (2004, [47]). This allows a decrease in size, weight and contamination risk for future RHU generations.

The utilization of radioisotope heating sources however entails the installation of a thermal control mechanism in the exploration robots, which consequently increases complexity, weight and cost of the system, as the possibility of overheating must be antagonized. Radioactive contamination risk in the event of an accident, or on the installed sensors (e.g. radiation sensors), must also be evaluated.

Chapter 7

Summary and Conclusions

In the present study the feasibility of a proposed thermal control architecture for planetary and lunar (sub-)surface exploration robots is demonstrated. The first order proof of concept relies on a low emissive surface finish to limit radiation heat losses and a low conductive insulation layer to limit convection heat losses when necessary and increase structure stability.

This enables a single, unique design to be employed for all envisioned mission destinations, as the projected heat loss never surpasses the internal heat generation. The universal architecture allows the robots to be deployed in a very flexible manner and thus reduces development costs.

Further observations and conclusions of the developed first order approximated numerical model are found in Section 5.5.

With one third of the robot mass being made up of fuel, which is a reasonable amount for space applications, long enough mission durations for viable mission scenarios are obtained.

The Moon is looked at as a first possible mission site for the exploration robots, as funding appears to be most easily acquirable due to a need in reconnaissance and mapping in view of future planned human deployment. The proposed mission concept would allow several advantages compared to a traditional rover mission, mainly due to less restricted mobility restraints, especially in caves and heavily cratered terrain. Such a mission would set the stage for later life detection missions, for example on Mars or Jupiter's Galilean Moons.

The decision on a thermal control mechanism installation must be carefully evaluated. As the majority of the proposed concepts and components must still be developed to meet specifications, in essence a curved Variable Emittance Coating surface and a small lightweight heat switch, a thorough analysis must be conducted. Because the use of a thermal control provision has a direct influence on system cost, weight, complexity, energy requirement and mission flexibility, all these effects must be included in the study to see if such a system is worthwhile installing and pursuing.

7.1 Outlook

In addition to a future study on the necessity of a thermal control mechanism, other suggestions for the pursuit of a realizable thermal control architecture are

enumerated in the following. In view of the 10 to 40-year project time frame and the early mission development stage, solely the most relevant are listed.

- The advantages and disadvantages resulting from the installation of a Radioisotope Heating Unit to increase the robot lifespan must be evaluated with respect to system cost, weight, complexity and science data gathering mission achievement.

- Once all internal robot components are exactly known, namely mobility actuators, energy generators and sensors, a detailed heat transfer model must be developed taking all into account. By means of a Finite Element Modeling (FEM) simulation the exact robot heat loss is determined in all imaginable and probable conditions. Potential holes in the shell structure and insulation layer for sensors, as well as robot modularity for individual configuration, must also be accounted for. After this, the exact specifications for the robots are defined.

- The cruise stage of the mission must further be analyzed. Particularly on how to keep the robots warm during a months or years-long cruise phase before reaching the designated planet or moon for exploration. A robot hibernation state during this time would make the most sense, to save fuel cell fuel. Heat can be provided during this time from the robot containing exterior.

- In particular on the Moon, and eventually on Mars, solar cell technology can be envisioned to provide additional energy to the exploration robots. On all other mission locations solar irradiation is too faint. Solar energy could be used on the Martian or lunar surface for mobility purposes and save fuel cell energy specifically for cave environments. Effects of increased complexity, high surface emissivities, time of day operation restrictions and required energy generation must however be studied in detail to assess the concept.

- In general, future technology developments also have to be kept an eye on, such as for example low temperature die attachments in electronics, researched by Kirschman *et al.* (2001, [48]), to increase Allowable Flight Temperatures (AFT).

Appendix A

Appendix

A.1 List of Symbols

α	Thermal diffusivity
β	Expansion coefficient
γ	Ratio inoperative to operative state
ΔT_b	Body temperature increase after 1 hour of heating
ϵ_s	Robot shell surface emissivity
$\epsilon_{s,vec}$	Apparent Variable Emittance Coating surface emissivity
η_{fc}	Fuel cell efficiency
η_{inc}	Fuel cell efficiency increase with thermoelectric generator
η_{te}	Maximal thermoelectric generator efficiency
η_{tot}	Overall robot heat to mechanical energy efficiency
λ	Thermal conductivity of surrounding gas
λ_{in}	Thermal conductivity of insulation layer
λ_{sw}	Switch thermal conductivity
μ	Dynamic viscosity of surrounding gas
μ_s	Surrounding gas dynamic viscosity at shell temperature
ν	Kinematic viscosity of surrounding gas
ρ	Density
$(\rho \cdot c_p)_b$	Density and heat capacity product of robot body
σ	Stefan-Boltzmann constant
χ	Mission duration reduction by thermal control provison
A_∞	Enclosure area
A_{cont}	Contact area of robot with supporting surface
A_s	Robot shell surface area
A_{sw}	Heat switch contact area
A_{vec}	Variable Emittance Coating surface area
$\overline{c}$	Mean particle velocity
c_p	Specific heat capacity at constant pressure
c_{p,CO_2}	Specific heat capacity at constant pressure for CO_2
c_{p,N_2}	Specific heat capacity at constant pressure for N_2

Table A.1: List of symbols (Part I)

c_v	Specific heat capacity at constant volume
d	Particle diameter in atmospheric gas
D	Robot diameter
D_b	Robot body diameter
d_{CO_2}	Carbon dioxide molecule diameter
d_{N_2}	Dinitrogen molecule diameter
E_{jump}	Fuel energy required for one hop
f	Arbitrary function
$\mathcal{F}_{s\infty}$	Configuration factor from robot shell surface to enclosure
g	Gravitational acceleration
g_{mars}	Gravitational acceleration on Mars
Gr_D	Grashof number for spherical body
g_{titan}	Gravitational acceleration on Titan
h	Heat transfer coefficient
HHV_{H_2}	Hydrogen higher heating value
I_{sun}	Incoming solar radiative flux
Kn	Knudsen number
l	Particle mean free path
m	Robot mass
M	Molecular mass
Max_{hops}	Maximum number of robot hops
M_{CO_2}	Carbon dioxide molecular mass
M_{H_2}	Dihydrogen molecular mass
m_{H_2}	Hydrogen mass
M_{N_2}	Dinitrogen molecular mass
M_{O_2}	Dioxygen molecular mass
m_{O_2}	Oxygen mass
M_{te}	Variable in thermoelectric efficiency calculation
n	Particles per unit volume
N_A	Avogadro number
$\overline{Nu_D}$	Nusselt number for a spherical body
$\overline{Nu_{D,forced}}$	Nusselt number for a spherical body in forced convection
$\overline{Nu_{D,free}}$	Nusselt number for a spherical body in free convection
p	Pressure
p_{mars}	Pressure on Mars
Pr	Prandtl number
p_{titan}	Pressure on Titan
$\dot{Q}_{cond,g}$	Conductive heat loss to ground
$\dot{Q}_{cond,s}$	Conductive heat loss through insulation layer to shell
$\dot{Q}_{cond,sw}$	Conductive heat loss through heat switch
$\dot{Q}_{conv}$	Convective heat loss
$\dot{Q}_{fc}$	Fuel cell energy production
$\dot{Q}_{heat,fc}$	Fuel cell heat production
$\dot{Q}_{loss}$	Overall robot heat loss to surroundings
$\dot{Q}_{loss,av}$	Average overall robot heat loss
$\dot{Q}_{rad}$	Radiative heat loss

Table A.2: List of symbols (Part II)

$\dot{Q}_{rad,vec}$	Radiative heat loss with Variable Emittance Coating
$\dot{Q}_{sun}$	Absorbed solar irradiation
r	Distance from celestial body to sun
R	Universal gas constant
Ra_D	Rayleigh number for spherical body
Re_D	Reynolds number for spherical body
r_s	Radius of sun
t	Time
T	Temperature
T_∞	Surrounding temperature
T_b	Body temperature
$T_{b,AFTmax}$	Minimum body Allowable Flight Temperature
$T_{b,AFTmin}$	Maximum body Allowable Flight Temperature
T_{hot}	Maximal celestial body surface temperature
$t_{mission}$	Robot mission duration
t_{max}	Maximum heating time within AFT limits
T_s	Shell surface temperature
T_{sun}	Sun temperature
u_{mars}	Maximal wind velocity on Mars
u_{titan}	Maximal wind velocity on Titan
x	Insulation thickness
x_{sw}	Heat switch length
Z	Thermoelectric Figure of Merit

Table A.3: List of symbols (Part III)

A.2 List of Abbreviations

AFT	Allowable Flight Temperature
AU	Astronomical Units
CPFC	Coated Particles Fuel Compact
EPAM	Electroactive Polymer Actuator Muscle
ESA	European Space Agency
ESR	Electrostatic Switched Radiator
ETH	Eidgenössische Technische Hochschule, Zurich
FEM	Finite Element Modeling
JAXA	Japan Aerospace Exploration Agency
JPL	Jet Propulsion Laboratory
LAN	Local Area Network
LWRHU	Light Weight Radioisotope Heating Unit
MEMS	Micro Electro-Mechanical System
MER	Mars Exploration Rover
MIT	Massachusetts Institute of Technology
NASA	National Aeronautics and Space Administration
NIAC	NASA Institute for Advanced Concepts
RHU	Radioisotope Heating Unit
RTG	Radioisotope Thermoelectric Generator
VEC	Variable Emittance Coating
WEB	Warm Electronics Box

Table A.4: List of abbreviations

A.3 *Mathematica* Source Code

Thermal Design Architecture

--- Modeling

Assumptions
- Spherical Shapes
- Isothermal Body
- Homogeneous Body
- Uniform Heat Production
- Uniform and Constant Outer Temperature
- Outer Temperature Equal to Supporting Surface Temperature
- Inner Insulation Surface Temperature at Body Temperature
- Steady State for Heat Transfer Analyses
- Surface Contact Area Temperature Identical to Outer Temperature
- Switch Either "On" or "Off"

Variables

- **Outer Temperature**

```
Tinfty = 50;
```

- **Distance Celestial Body - Sun**

```
r = 1.52366;
```

- **Atmospherical Conditions on Celestial Body**

- **Gravity**

```
g = 3.71;
```

- **Atmospheric Pressure**

```
p = 750;
```

- **Wind Speed**

```
u = 20;
```

- **Gas Molecular Weight**

```
M = 44 * 10^-3;
```

- **Particle Diameter**

```
d = 3.32 * 10^-10;
```

Figure A.1: *Mathematica* Source Code (Page 1)

- **Specific Heat**

```
cp = 27.437 + 4.2315 * 10^-2 * Tinfty - 1.9555 * 10^-5 * Tinfty^2 + 3.9968 * 10^-9 * Tinfty^3 - 2.9872 * 10^-13 * Tinfty^4;
```

Set Variables

- **Diameter of Shell**

```
Ds = 0.10;
```

- **Diameter of Body**

```
Db = 0.05;
```

- Required density for 100g: ca. 1500 kg/m3

- **Body Temperature**

```
Tb = 300;
```

- **Body AFT Limits**

```
Tminaft = 233;
Tmaxaft = 313;
```

- **Body Density and Heat Capacity Product**

```
ρcp = 3 * 10^6;
```

- **Insulation Thickness**

```
x = 0.025;
```

- **Thermal Conductivity of Insulation**

```
λin = 0.005;
```

- **Emissivity of Shell**

```
εs = 0.01;
```

- **Contact Area with Surface**

```
Acont = 0.01^2;
```

- **Fuel Cell Heat Production**

```
Qfc = 1;
```

- **Fuel Cell Efficiency**

```
ηfc = 0.65;
```

- **Overall Energy Effiency**

```
ηtot = 0.02;
```

Figure A.2: *Mathematica* Source Code (Page 2)

- **Required Energy per Hop**

```
He = 0.6;
```

- **Maximum Amount of Hops**

```
Hmax = 15000;
```

- **Relative Area of VEC on Shell**

```
Avec = 0.75;
```

- **Thermoelectric Figure of Merit**

```
Z = 3 * 10^-3;
```

- **Length of Thermal Swich**

```
xsw = 0.03;
```

- **Contact Area of Thermal Switch**

```
Asw = 0.0015^2;
```

- **Configuration Factor**

```
F = 1;
```

Constants and Operations

```
<< Graphics`Graphics`
```

- **Reset Variables**

```
Ts =.
```

- **Constants**

```
σ = 5.67 * 10^-8;
R = 8.314;
NA = 6.022 * 10^23;
Vb = 4 / 3 * π * (Db / 2)^3;
As = 4 * π * (Ds / 2)^2;
AU = 1.4959787006 * 10^11;
```

- **Semimajor Axis Length**

```
r = r * AU;
```

- **Radiation Heat Loss**

```
Qrad = σ * εs * As * (Ts^4 - Tinfty^4) * F;
```

Figure A.3: *Mathematica* Source Code (Page 3)

- **Conduction Heat Loss**

```
Qconds = 4 * π * λin * (Tb - Ts) / (1/(Ds/2 - x) - 1/(Ds/2));
Qcondg = Acont * λin * (Tb - Tinfty) / x;
```

- **Convection Heat Loss**

```
ρ = (p * M) / (R * Tinfty);
c = ((8 * R * Tinfty) / (π * M)) ^ (0.5);
l = (R * Tinfty) / (√2 * π * d^2 * NA * p);
μ = 1 / 3 * ρ * c * l;

ρs = (p * M) / (R * Ts);
cs = ((8 * R * Ts) / (π * M)) ^ (0.5);
ls = (R * Ts) / (√2 * π * d^2 * NA * p);
μs = 1 / 3 * ρs * cs * ls;

ν = μ / ρ;
cv = cp - R;
λ = (p / (R * Tinfty)) * c * l * cv / 3;

cpsi = cp / M;
cvsi = cv / M;
α = λ / (ρ * cpsi);

β = 1 / Tinfty;
Ra = (g * β * (Ts - Tinfty) * Ds^3) / (ν * α);
Pr = ν / α;
Nufree = 2 + (0.589 * Ra^0.25) / (1 + (0.469 / Pr)^(9/16))^(4/9);
hfree = Nufree * λ / Ds;
Qconvfree = hfree * As * (Ts - Tinfty);

Rey = u * Ds / ν;
(*Nuforced=2+(0.4*Rey^0.5+0.06*Rey^(2/3)) Pr^0.4 (μ/μs)^0.25;*)
Nuforced = 2 + (0.4 * Rey^0.5 + 0.06 * Rey^(2/3)) Pr^0.4;
hforced = Nuforced * λ / Ds;
Qconvforced = hforced * As * (Ts - Tinfty);

Qconv = If[u == 0, Qconvfree, Qconvforced];
Qconv = If[p < 10, 0, Qconv];

Qconvapp = Qconv;
```

- **Qloss**

```
eq1 = Qs == Qconds;
eq2 = Qs == Qrad + Qconv;
res = NSolve[{eq1, eq2}, {Qs, Ts}];
Qshell = If[(u == 0 && p > 10), Qs /. res[[3]][[1]], Qs /. res[[4]][[1]]];
Ts = If[(u == 0 && p > 10), Ts /. res[[3]][[2]], Ts /. res[[4]][[2]]];
Qloss = Qshell + Qcondg;
```

- **Thermoelectrics**

```
Qheatfc = (1 - ηtot) * Qfc;
M = (1 + Z (Tb + Ts) / 2) ^ (0.5);
ηte = 0.5 * (Tb - Ts) / Tb * ((M - 1) / (M + (Ts / Tb)));
Wte = ηte * Qheatfc;
ηinc = ((ηfc + ηte) / ηfc - 1) * 100;
```

Figure A.4: *Mathematica* Source Code (Page 4)

- **Thot**

```
rs = 0.696 * 10^9;
Tsun = 5780;
Thot = Tsun * Sqrt[rs / r];
```

- **Solar Irradiation**

```
Isun = σ * Tsun^4 * (rs / r)^2;
Qsun = εs * 0.5 * As * Isun;
```

- **Transient Body Temperature Increase during Heating**

```
Tin = 300;
Qcondst = 4 * π * λin * (w[t] - Tst) / (1 / (Ds / 2 - x) - 1 / (Ds / 2));
Qradt = σ * εs * As * (Tst^4 - Tinfty^4) * F;

Rat = (g * β * (Tst - Tinfty) * Ds^3) / (ν * α);
Nut = 2 + (0.589 * Rat^0.25) / (1 + (0.469 / Pr)^(9/16))^(4/9);
ht = Nut * λ / Ds;
Qconvt = ht * As * (Tst - Tinfty);
Qconvt = If[p < 10, 0, Qconvt];

eq1 = Qst == Qcondst;
eq2 = Qst == Qradt + Qconv;
res = NSolve[{eq1, eq2}, {Qst, Tst}];
Qshellt = Qst /. res[[3]][[1]];

Qcondgt = Acont * λin * (w[t] - Tinfty) / x;

Qlosst = Qshellt + Qcondgt;
Qlosssunt = Qshellt + Qcondgt - Qsun;

solution = NDSolve[{w'[t] == (Qheatfc - Qlosst) / (ρcp * Vb), w[0] == Tin}, w, {t, 0, 7200}];
solutionsun = NDSolve[{w'[t] == (Qheatfc - Qlosssunt) / (ρcp * Vb), w[0] == Tin}, w, {t, 0, 7200}];
deltaT = (w[t] /. solution[[1]] /. t → 3600) - Tin;
deltaTsun = (w[t] /. solutionsun[[1]] /. t → 3600) - Tin;
```

- **VEC**

```
Qradvec = As * σ * (εs * (1 - Avec) + εsvec * (Avec)) * (Tb^4 - Tinfty^4) * F;
εres = FindRoot[(Qradvec + Qcondg + Qconv) == Qheatfc, {εsvec, 0.02}];
εmin = εsvec /. εres;
εressun = FindRoot[(Qradvec + Qcondg + Qconv - Qsun) == Qheatfc, {εsvec, 0.02}];
εminsun = εsvec /. εressun;
```

- **Ratio Inop/Op State**

```
γ = Qheatfc / Qlossav;
```

- **Mission Duration Reduction by Thermal Control Provision**

```
χ = (1 - Qlossav / Qheatfc) * 100;
```

Figure A.5: *Mathematica* Source Code (Page 5)

- **Maximal Heating Time within AFT Limits**

```
solution = DSolve[{waft'[t] == (Qheatfc - Qlossav) / (ρcp * Vb), waft[0] == Tminaft}, waft, t];
Tfunc[t] = waft[t] /. solution[[1]];
solution = Solve[Tfunc[t] == Tmaxaft, t];
taft = t /. solution[[1]];
taft = taft / 3600;
```

- **Mission Range**

```
Ht = He / (Qfc * ηtot);
lmin = Hmax * Ht / (3600 * 24);
lmax1 = lmin / (1 - χ / 100);
lmax2 = Hmax * Ht / Qlossav / (3600 * 24);
```

Passive-Cold Case

Assumptions

- No Solar Irradiation (Cave, Night)
- Tb kept at 300K
- Qfc=0 (inop state)
- Max Output for TE

=>Goal: Qloss,max<Qheat,fc

Convective Heat Loss

```
Qconv
```

Radiative Heat Loss

```
Qshell - Qconv
```

Conductive Heat Loss into Ground

```
Qcondg
```

Total Heat Loss to Surroundings

```
Qloss
```

Surface Temperature

```
Ts
```

Efficiency Increase

```
ηinc
```

Figure A.6: *Mathematica* Source Code (Page 6)

Active-Hot Case

Assumptions
- Tb start at 300K
- Qfc=1

=>Goal: Qloss=0, ϵsvec<1, λsw<500

Maximal Temperature

```
Thot
```

Solar Irradiation

```
Isun
```

```
Qsun
```

Free Convection Heat Loss

```
Qconv
```

Transient Body Temperature Increase during Heating

Approximation: Convection Heat Loss constant over all times
(no further refinement supported by *Mathematica* in DE solution algorithm)

- **In cave**

```
deltaT
```

- **In sun**

```
deltaTsun
```

VEC - Radiative Heat Loss into Atomosphere

- **Plot**

```
Plot[Qradvec, {esvec, 0.01, 1}, AxesLabel → {"[ε]", "[Q]"}, ImageSize → 400];
```

- **VEC Emittance Specifications without Sun Influence**

```
emin
```

- **VEC Emittance Specifications with Sun Influence**

```
eminsun
```

Figure A.7: *Mathematica* Source Code (Page 7)

Thermal Switch - Conductivity Specifications

- **Mathematical Operations**

```
λinv =.;
λinres = Solve[(λinv * Asw * (Tb - Tinfty) / xsw) + Qloss == Qheatfc, λinv];
λinmin = λinv /. λinres[[1]];
λinressun = Solve[(λinv * Asw * (Tb - Tinfty) / xsw) + Qloss - Qsun == Qheatfc, λinv];
λinminsun = λinv /. λinressun[[1]];
```

- **Minimal Value of λin to Ensure Cooling without Sun Influence**

```
λinmin
```

- **Minimal Value of λin to Ensure Cooling with Sun Influence**

```
λinminsun
```

Mission Scenarios

Variables

```
Qlossav = 0.2;
```

Ratio Inop/Op State

```
ϒ
```

Mission Duration Reduction by Thermal Control Provision

```
χ
```

Maximal Heating Time within AFT Limits

```
taft
```

Maximal Duration

```
lmax2
```

Mission Range

- **Plot**

```
DisplayTogether[Plot[Hmax / lmin * th, {th, 0, lmin},
   AxesLabel → {"[Days]", "[Hops]"}, ImageSize → 400], Plot[Hmax, {th, lmin, lmax1}],
  Plot[-Hmax / (lmax2 - lmax1) * th + Hmax / (lmax2 - lmax1) * lmax2, {th, lmax1, lmax2}]];
```

Figure A.8: *Mathematica* Source Code (Page 8)

A.4 Moon Deployment Study

Analogous to the Mars deployment study in Section 6.6, the same can be done for the Moon, where an average heat loss of $\dot{Q}_{loss,av} = 0.1$ W is assumed. The results are found in Figure A.9.

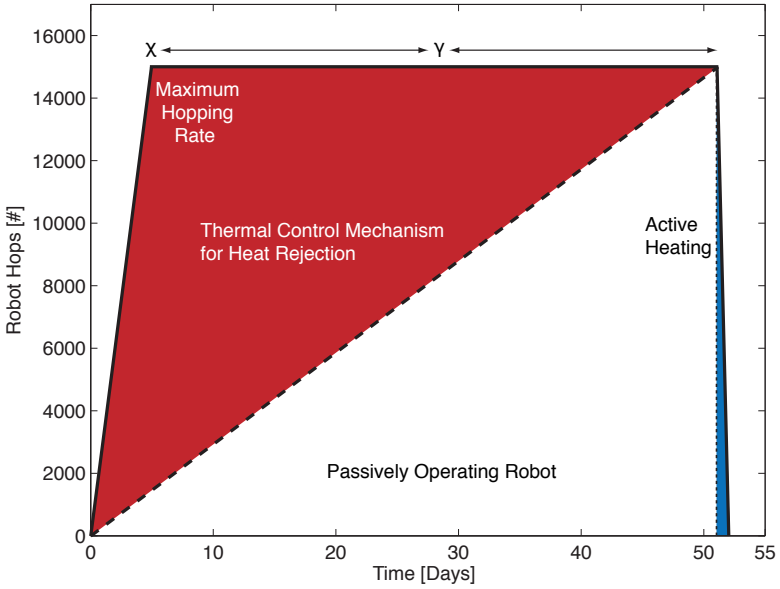

Figure A.9: Moon reference mission profile with $\dot{Q}_{loss,av} = 0.1$ W and 30 g of fuel on board

Bibliography

[1] The News Staff. Breakthrough of the Year: The Runners-Up. *Science*, 310(5756):1880–1885, December 2005.

[2] National Aeronautics and Space Administration. The Vision for Space Exploration. Technical report, NASA, February 2004.

[3] NASA Institute for Advanced Concepts. Annual Report. Technical report, NIAC, 2004.

[4] S. Dubowsky, K. Iagnemma, and P. J. Boston. Microbots for Large-Scale Planetary Surface and Subsurface Exploration. Technical report, NIAC Phase II Proposal, 2005.

[5] R. O'Hayre, D. Braithwaite, W. Hermann, S.-J. Lee, T. Fabian, S.-W. Cha, Y. Saito, and F. B. Prinz. Development of Portable Fuel Cell Arrays with Printed-Circuit Technology. *Journal of Power Sources*, 124:459–472, 2003.

[6] P. R. Weismann, L.-A. McFadden, and T. V. Johnson, editors. *Encyclopedia of the Solar System.* Academic Press, 1999.

[7] N. McBride and I. Gilmour, editors. *An Introduction to the Solar System.* Cambridge University Press, 2004.

[8] T. Z. Martin, N. T. Bridges, and J. R. Murphy. Near-Surface Temperatures at Proposed Mars Exploration Rover Landing Sites. *Journal of Geophysical Research*, 108(E12): Art. No. 8089, 2003.

[9] R. M. Haberle, M. Joshi, J. Murphy, J. Barnes, J. T. Schofield, G. Wilson, M. Lopez-Valverde, J. Hollingsworth, A. F. C. Bridger, and J. Schaeffer. General Circulation Model Simulations of the Mars Pathfinder Atmospheric Structure Investigation/Meteorology Data. *Journal of Geophysical Research*, 104:8957–8974, 1999.

[10] Jet Propulsion Laboratory (JPL) – NASA. Io Fact Sheet. http://www2.jpl.nasa.gov/galileo/io/fact.html, November 2005.

[11] Jet Propulsion Laboratory (JPL) – NASA. Europa Fact Sheet. http://www2.jpl.nasa.gov/galileo/europa/fact.html, November 2005.

[12] Jet Propulsion Laboratory (JPL) – NASA. Ganymede Fact Sheet. http://www2.jpl.nasa.gov/galileo/ganymede/fact.html, November 2005.

[13] Jet Propulsion Laboratory (JPL) – NASA. Callisto Fact Sheet. http://www2.jpl.nasa.gov/galileo/callisto/fact.html, November 2005.

[14] G. S. Hickey, D. Braun, L.-C. Wen, and H. J. Eisen. Integrated Thermal Control for Mars Rover. Technical report, NASA Jet Propulsion Laboratory, 1996.

[15] K. S. Novak, C. J. Phillips, G. C. Birur, E. T. Sunada, and M. T. Pauken. Development of a Thermal Control Architecture for the Mars Exploration Rovers. In *Proceedings of the 2003 Space Technology and Applications International Forum (STAIF-2003)*, Albuquerque, NM, U.S.A., February 2003.

[16] K. S. Novak, C. J. Phillips, E. T. Sunada, and G. M. Kinsella. Mars Exploration Rover Surface Mission Flight Thermal Performance. In *Proceedings of the 35^{th} International Conference on Environmental Systems*, SAE Technical Paper Series Number 2005-01-2827, Rome, Italy, 2005.

[17] M. Pauken, E. Sunada, K. Novak, C. Phillips, G. Birur, and K. Lankford. Development Testing of a Paraffin-Actuated Heat Switch for Mars Rover Applications. In *32^{nd} International Conference on Environmental Systems*, San Antonio, TX, U.S.A., 2002.

[18] G. H. Rinehart. Design Characteristics and Fabrication of Radioisotope Heat Sources for Space Missions. *Progress in Nuclear Energy*, 39(3–4):305–319, 2001.

[19] European Space Agency. Lessons Learnt from Beagle 2 and Plans to Implement Recommendations from the Commision of Inquiry. Press release, ESA, May, 2004.

[20] T. S. Swanson and G. C. Birur. NASA Thermal Control Technologies for Robotic Spacecraft. *Applied Thermal Engineering*, 23:1055–1065, 2003.

[21] W. Biter, S. Hess, S. Oh, D. Douglas, and T. Swanson. Electrostatic Radiator for Satellite Temperature Control. In International Institute of Electrical and Electronics Engineers, editors, *Proceedings of 2005 IEEE Aerospace Conference*, Piscataway, NJ, U.S.A., April 2005.

[22] J. H. Lienhard IV and J. H. Lienhard V. *A Heat Transfer Textbook*. Phlogiston Press, 3rd edition, 2005.

[23] Yu. K. Akimov. Fields of Application of Aerogels (Review). *Instruments and Experimental Techniques*, 46(3):287–299, 2003.

[24] D. Lee, P. C. Stevens, S. Q. Zeng, and A. J. Hunt. Thermal Characterization of Carbon-Opacified Silica Aerogels. *Journal of Non-Crystalline Solids*, 186:285–290, 1995.

[25] K. E. Parmenter and F. Milstein. Mechanical Properties of Silica Aerogel. *Journal of Non-Crystalline Solids*, 223:179–189, 1998.

[26] M. Reim, G. Reichenauer, W. Körner, J. Manara, M. Arduini-Schuster, S. Korder, A. Beck, and J. Fricke. Silica-Aerogel Granulate - Structural, Optical and Thermal Properties. *Journal of Non-Crystalline Solids*, 350:358–363, 2004.

[27] R. Osiander, S. L. Firebaugh, J. L. Champion, D. Farrar, and M. A. Garrison Darrin. Microelectromechanical Devices for Satellite Thermal Control. *IEEE Sensors Journal*, 4(4):525–531, 2004.

[28] W. Biter, S. Oh, and S. Hess. Electrostatic Switched Radiator for Space Based Thermal Control. In Americain Institute of Physics, editor, *Proceedings of the 2002 Space Technology and Applications International Forum (STAIF-2002)*, Albuquerque, NM, U.S.A., February 2002.

[29] W. Biter, S. Hess, and S. Oh. Electrostatic Radiator for Spacecraft Temperature Control. In Americain Institute of Physics, editor, *Proceedings of the 2004 Space Technology and Applications International Forum (STAIF-2004)*, Albuquerque, NM, U.S.A., February 2004.

[30] D. Farrar, W. Schneider, R. Osiander, J. L. Champion, A. G. Darrin, D. Douglas, and T. D. Swanson. Controlling Micro Electro Mechanical Systems (MEMS) in Space. In Americain Institute of Physics, editor, *Proceedings of the 2003 Space Technology and Applications International Forum (STAIF-2003)*, Albuquerque, NM, U.S.A., February 2003.

[31] F. H. Milanez and M. B. H. Mantelli. Theoretical and Experimental Studies of a Bi-metallic Heat Switch for Space Applications. *International Journal of Heat and Mass Transfer*, 46(24):4573–4586, 2003.

[32] T. Slater, P. Van Gerwen, E. Masure, F. Preud'homme, and K. Baert. Thermomechanical Characteristics of a Thermal Switch. *Sensors and Actuators A: Physical*, 53(1-3):423–427, 1996.

[33] J.-S. Plante. Ball Robot Mobility System Specifications. Technical report, Field and Space Robotics Laboratory, MIT, 2005.

[34] M. F. Modest. *Radiative Heat Transfer*. Academic Press, 2003.

[35] R. Siegel and J. R. Howell. *Thermal Radiation Heat Transfer*. Taylor & Francis, 2002.

[36] F. P. Incropera and D. P. DeWitt. *Fundamentals of Heat and Mass Transfer*. John Wiley & Sons, 1996.

[37] G. Chen. *Nanoscale Energy Transport and Conversion: A Parallel Treatment of Electons, Molecules, Phonons, and Photons*. MIT-Pappalardo Series in Mechanical Engineering. Oxford University Press, 2005.

[38] J. Kestin and J. R. Dorfman. *A Course in Statistical Thermodynamics*. Academic Press, 1971.

[39] C. Kittel and H. Kroemer. *Thermal Physics*. W. H. Freeman and Company, 1980.

[40] D. M. Rowe. Applications of Nuclear-Powered Thermoelectric Generators in Space. *Applied Energy*, 40:241–271, 1991.

[41] D. M. Rowe, editor. *CRC Handbook of Thermoelectrics*. CRC Press, LLC, 1995.

[42] G. S. Nolas. *Thermoelectrics: Basic Principles and New Materials Developments*. Springer, 2001.

[43] D. Kaplan. Environment of Mars, 1988. In *NASA Technical Memoradum 100470*, Lyndon B. Johnson Space Center, Houston, TX, U.S.A., October 1988.

[44] D. R. Lide, editor. *CRC Handbook of Chemistry and Physics*. CRC Press, LLC, 2004.

[45] C. L. Yaws, editor. *Chemical Properties Handbook*. McGraw-Hill, 1999.

[46] J. H. Saleh, J.-P. Torres-Padilla, D. E. Hastings, and D. J. Newan. To Reduce or to Extend a Spacecraft Design Lifetime? *Journal of Spacecraft and Rockets*, 43(1):207–217, 2006.

[47] M. S. El-Genk and J.-M. Tournier. An Analysis of Coated Particles Fuel Compact-General Purpose Heat Source (CPFC-GPHS). *Progress in Nuclear Energy*, 44(3):215–236, 2004.

[48] R. K. Kirschman, W. M. Sokolowski, and E. A. Kolawa. Die Attachment for -120°C to +20°C Thermal Cycling of Microelectronics for Future Mars Rovers - An Overview. *Journal of Electronic Packaging*, 123:105–111, 2001.